Chemometrics evaluation of phase transformations based on ATR-IR spectra and powder X-ray diffractogram.

2018

Yuta Otsuka

1. Introduction

1.1 ATR-IR spectroscopy

Vibrational spectroscopies are extensively used for the characterization of materials in various academic and industrial fields. A vibration is defined as periodic variation of the interatomic distance in a compound. In the case of a diatomic molecule, A-B, the vibration frequency is modeled using the simple Hook's law under the approximation of a harmonic oscillator. The frequency of vibration ν is defined as the following equation:

$$\nu = \frac{1}{2\pi c}\sqrt{\frac{\kappa}{\mu}} \qquad (1\text{-}1)$$

where κ is the force constant associated with the chemical bond and μ is the reduced mass. For more complicated molecules, different types of vibrations are possible [1]. Two types of vibrations with different energy are recognized for the molecules other than diatomic ones: stretching vibration ν, corresponding to an elongation of chemical bonds, and bending vibration. The later exhibits higher energy than the former.

Infrared spectroscopy is an analytical technique that offers various applications in the field of pharmaceutical sciences. Fourier transform (FT) – IR spectroscopy, which is widely employed in scientific researches, requires sample dilution with KBr powder, because its sensitivity is too high to measure raw materials [2]. In contrast, attenuated total reflectance (ATR) – IR spectroscopy enables rapid and nondestructive measurements of as low as few mg of solid and liquid samples either in bulky or filmy state without any dilution. Moreover, ATR-IR spectroscopy can analyze suspension and paste samples.

1.2 Apatite cement

The continuous development of biocompatible materials has got attention to the application of different forms of calcium phosphate derivatives. Amongst them, hydroxyapatite (HAp) has been proven to be biocompatible, chemically stable and can be used for a wide range of bone-related applications. The focus of current researches is to

develop more biologically simulated versions of HAp.

Although the inorganic constituent of bone is recognized as HAp [3], biological HAp is, more strictly, a carbonate apatite expressed as the chemical formula of $Ca_{10-a}(PO_4)_{6-b}(CO_3)_b(OH)_{2-c}$. In the carbonate apatite, CO_3^{2-} substitutes for the lattice ion of HAp (*i.e.,* PO_4^{3-} or OH^-) [4]. Brown and Chow reported that the mixture of metastable calcium phosphates, tetracalcium phosphate (TeCP) and dicalcium phosphate dihydrate (DCPD), transformed into HAp with similar crystallinity to that of bone [5]. Thus formed "self-setting TeCP-DCPD apatite cement" hardens isothermally around neutral pH, enabling the inclusion of drugs such as insulin and cephalexin without denaturation. The cement is capable of inducing massive osteoconduction and replaced by the host bone when it is embedded in bone [6].

1.3 Polymorphism

The polymorphs and pseudo-polymorphs (hydrates and solvates) of pharmaceuticals exhibit different physicochemical properties such as solubility, dissolution rate, stability and hygroscopicity. They also relate to the variation of pharmaceutical properties of dosage forms, *e.g.*, bioavailability, efficacy, stability and toxicity [7]. Pharmaceutical regulations are, therefore, required for the production of an appropriate bulk powders, in which well specified crystalline modifications are included [8]. Hygroscopic compounds in a solid dosage form often come in contact with moisture stemmed from manufacturing and/or storage processes, resulting in the polymorphic transformation [9].

Powder X-ray diffraction analysis (PXRD) is the most popular and useful method to identify crystalline modifications and to determine respective contents in bulk powders and/or excipients for pharmaceutical preparations, as regulated in United States Pharmacopeia and the Japanese Pharmacopeia [10]. However, PXRD needs more time for drying and analyzing sample. ATR-IR spectroscopy can, therefore, be employed as an alternative method to analyze crystallinity or crystal structure instead of PXRD [11].

1.4 Chemoinformatics

Chemoinformatics is a useful tool to analyze complex data (*e.g.*: spectra, chromatograms, X-ray diffractograms). The most widely used chemoinformatic methods include multiple linear regression, principal component analysis / principal component

regression (PCA/PCR) and partial least squares (PLS) regression [12]. The multivariate curve resolution (MCR) – alternating least squares (ALS) method can provide an improved resolution compared to other methods, and allow quantitative determinations [13]. Calvo *et al.* reported the effect of temperature on the cimetidine crystal transition (Form A, B, C, D and mono hydrate) based on ATR-IR spectroscopy and MCR-ALS [14].

Regulatory authorities such as the United States Food and Drug Administration and the International Conference on Harmonization have requested to use application process analysis tool of quality of the medicine in order to reduce the production risk of inferior pharmaceuticals [15,16]. Since the introduction of guidelines for process analytical technology (PAT), on-line and real-time analysis as a tool for monitoring and controlling manufacturing process has become increasingly accepted in pharmaceutical industry [17,18].

2. Effect of carbon dioxide on self-setting apatite cement formation from tetracalcium phosphate and dicalcium phosphate dihydrate; ATR-IR and chemoinformatics analysis

2.1 Introduction

Hydroxyapatite ($Ca_{10}(PO_4)_6(OH)_2$; HAp) (more strictly, non-stoichiometric substituted HAp) is a major constituent of bone (~60% by weight) and has high biocompatibility. In the field of biomaterials, bioactive HAp bone cements are generally produced from tetracalcium phosphate ($Ca_4(PO_4)_2O$; TeCP) and dicalcium phosphate dihydrate ($CaHPO_4 \cdot 2H_2O$; DCPD) in the presence of phosphoric acid. This kind of bone cement, which contains remaining TeCP and DCPD, is called "self-setting apatite cement (SSAC)". The cement has moderate crystallinity with similar characteristics to mammalian bone [5,19,20] and high biocompatibility. It is often used as a bone filler for bone defects in orthopedic surgery [21]. Hamanishi *et al.* reported a new drug delivery system (DDS) for Vancomycin, based on SSAC; the DDS-SSAC was successfully applied to the treatment of methicillin resistant *Staphylococcus auresus* osteomyelitis [6]. Hamada *et al.* reported a DDS-SSAC containing simvastatin, and the medium-responsive release of the drug *in vitro*. They investigated bone mineral density change after the implantation of the DDS-SSAC in osteoporotic rats by means of an X-ray computed tomography [22].

Miyamoto *et al.* quantitatively measured the transformation of TeCP and dicalcium phosphate anhydrate (DCPA) into HAp by a powder X-ray diffraction analysis (XRD) [23]. XRD is, however, not sufficient to measure the self-setting process, because XRD cannot follow rapid reaction in minutes or shorter. In addition, the method requires relatively large amount of sample (> 0.1 g). It is, therefore, highly desirable to clarify the self setting mechanism of HAp from TeCP, DCPD (or DCPA) in order to develop new generation biomaterials.

Fourier transform infrared (FT-IR) spectroscopy is one of the most versatile analytical methods for the identification of materials and the quantification of their components. The spectroscopy can afford chemical and/or physical information on the materials with IR-active vibrations (symmetrical/anti-symmetrical stretching, scissoring, *etc.*), light diffusivity and so on. The relationship between IR absorbance and the concentration of the component obeys Lambert-Beer's law. Petrov and Šoptrajanov

successfully applied FT-IR spectroscopy to the characterization of metastable calcium phosphates [24]. Changa and Tanaka [25] employed FT-IR spectroscopy to analyze the cross-linking of the HAp/Collagen nano-composite. Conventional FT-IR spectroscopy requires, however, sample dilution with potassium bromide powder, because its sensitivity is too high to measure raw materials. Attenuated total reflection (ATR)-IR spectroscopy can overcome such shortcomings of FT-IR spectroscopy, and rapidly measure a few milligrams of sample in monolithic, thin film-like or liquid form without dilution [26,27].

Chemoinformatics is a combination of mathematical and statistical methods for the design or selection of the optimal conditions of experiments and for the derivation of utmost pieces of chemical information through the analysis of acquired data [28,29]. Principal component analysis (PCA) is a multivariate analysis that can be used for the analyses of reaction kinetics and of spectra obtained by spectroscopies [14].

The author has been studying on the polymorphic transition of drugs in pharmaceutical tablet by means of XRD [9] or FT-near infrared spectroscopy coupled with Chemoinformatics [31]. In the present study, the author proposed an ATR-IR and PCA based approach for the elucidation of the reaction mechanism of rapid self-setting apatite formation from TeCP-DCPD suspension.

2.2 Experimental

2.2.1 Materials

TeCP and DCPD powders were purchased from Taihei Chemical Industrial Co. (Osaka, Japan) and Wako Pure Chemical Industries (Osaka, Japan), respectively. The apatite cement was prepared according to the procedure described by Brown and Chow [5]. The raw material for the preparation of the cement powder was an equimolar mixture of TeCP and DCPD powders, in which the molar ratio of Ca/P was 1.67.

2.2.2 Powder X-ray diffraction analysis

The raw material, which had been stored at high humidity, was carefully ground in an agate mortar with a pestle. Loosely packed sample was prepared in order to avoid crystal orientation when it was poured in the holder of the instrument without compression. The crystal phases in the specimens thus prepared were analyzed with a powder X-ray diffraction (XRD) system (Miniflex Rigaku Co. Ltd., Tokyo, Japan) at room temperature. Measurement conditions were as follows: Ni-filtered CuKα radiation (λ = 0.1540 nm); voltage, 30 kV; current, 15 mA; time constant, 1 s; step slit, 0.2°; counting time, 1.0 s; measurement range, 2θ = 5.0° ~ 45.0°.

2.2.3 Infrared spectroscopy measurement

Infrared spectra were measured with an FT-IR spectrometer (FT/IR-6500, JASCO Co., Tokyo, Japan) equipped with an ATR accessory, which was inserted directly in the light beam. Five milligrams of mixed TeCP-DCPD powder was kneaded with 20.0 μL of 11.0 mmol/L phosphoric acid. The paste was put on a germanium glass of the ATR accessory and covered with a sheet of Parafilm® at room temperature. IR spectra of the suspensions were measured in the range of 600–3800 cm^{-1} at a resolution of 8 cm^{-1} and acquired as digital data in a computer for further kinetic analysis. The data of 120 scans were normalized based on the area under the observed spectrum [32] and corrected, where air spectrum was subtracted from the averaged spectrum as a background.

2.2.4 Software

The chemoinformatics calculations were performed by UNSCRAMBLER software version 10.2 from CAMO (Computer Aided Modelling, Trondheim, Norway).

2.2.5 Principal component analysis (PCA)

Although ATR-IR spectra can be represented in n-dimensional space, it is

difficult to comprehend the data in the dimensions more than three. It is, therefore, useful to reduce the dimensionality of the multidimensional spectral space [33]. Multivariate analysis methods such as PCA can reduce the dimensionality of multidimensional space while retaining most of the original information in the data set. PCA operates by obtaining eigenvalues of the variance-covariance matrix (S) of the origin of data set and the eigenvectors. Calculation of the eigenvalues and eigenvectors can be accomplished readily *via* the singular value decomposition of S. The mean centered data matrix X is, therefore, reduced to the sum of a cross-product of two smaller matrixes P and T, and a residual matrix E,

$$X = TP^T + E \tag{2-1}$$

Where T is the matrix of the eigenvectors (loadings) and P is the matrix of scores. The cross-product of TP^T contains most of the original variance in X. This term (TP^T) is the structured part of the data: the part that is most informative. The remain (E) represents the fraction of variation that cannot be modelled well [32].

2.3 Results and discussion

2.3.1 XRD analysis

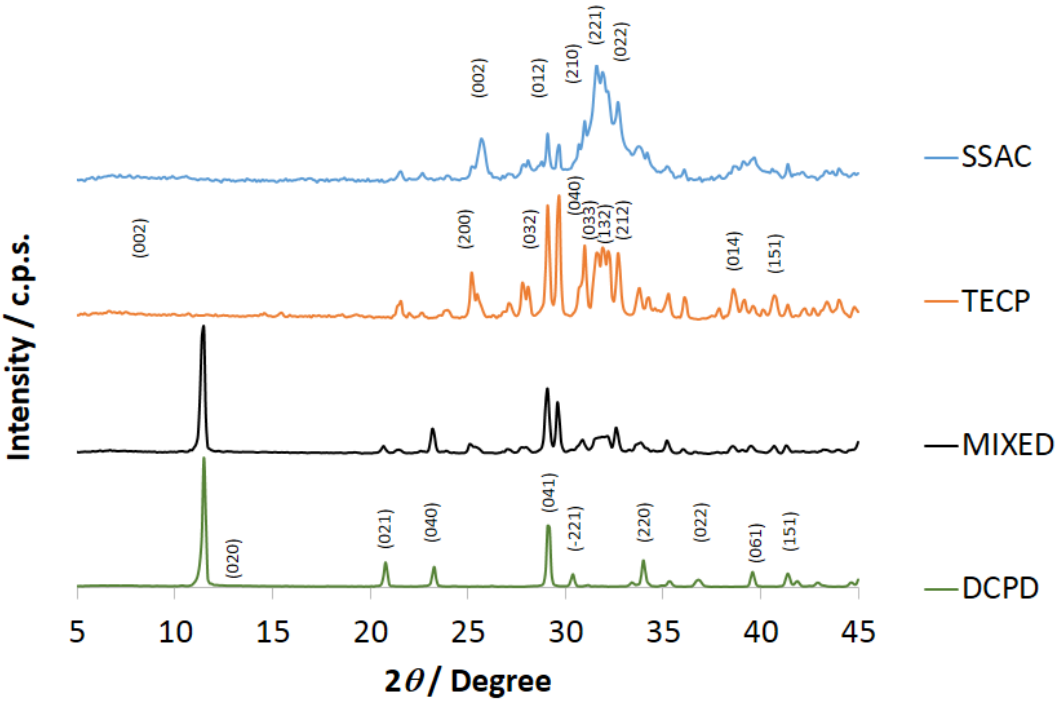

Fig. 2-1 XRD profiles of apatite cement before and after setting.
MIXED: equimolar mixture of TeCP and DCPD before the setting.
SSAC: self setting apatite cement.

Fig. 2-1 shows the powder X-ray diffractograms of SSAC, TeCP, equimolar mixture of DCPD and TeCP raw cement, and DCPD; SSAC was prepared through kneading the TeCP-DCPD mixture (5.0 g) with 11.0 mmol/L phosphoric acid (20.0 μL) for one day. The profile of SSAC shows broad peaks at 25.8, 31.6 and 32.7° that are characteristic of HAp. The profile of TeCP have distinct peaks at 25.2, 27.8, 28.1, 29.1, 29.6, 31.0, 32.1, 33.8, 35.3, 36.1, 38.6 and 40.8°. That of DCPD does so at 11.5, 20.8, 23.3, 29.2, 30.4, 34.0, 39.6 and 41.5°. These results indicate that the bulk powder of TeCP-DCPD mixture transform into HAp, but very small amounts of DCPD (2θ = 29.2°) and TeCP (2θ = 25.2°) are remained. Similar results were reported by Hayakawa *et al.* [34] and Otsuka *et al.* [35].

2.3.2 ATR-IR spectroscopy

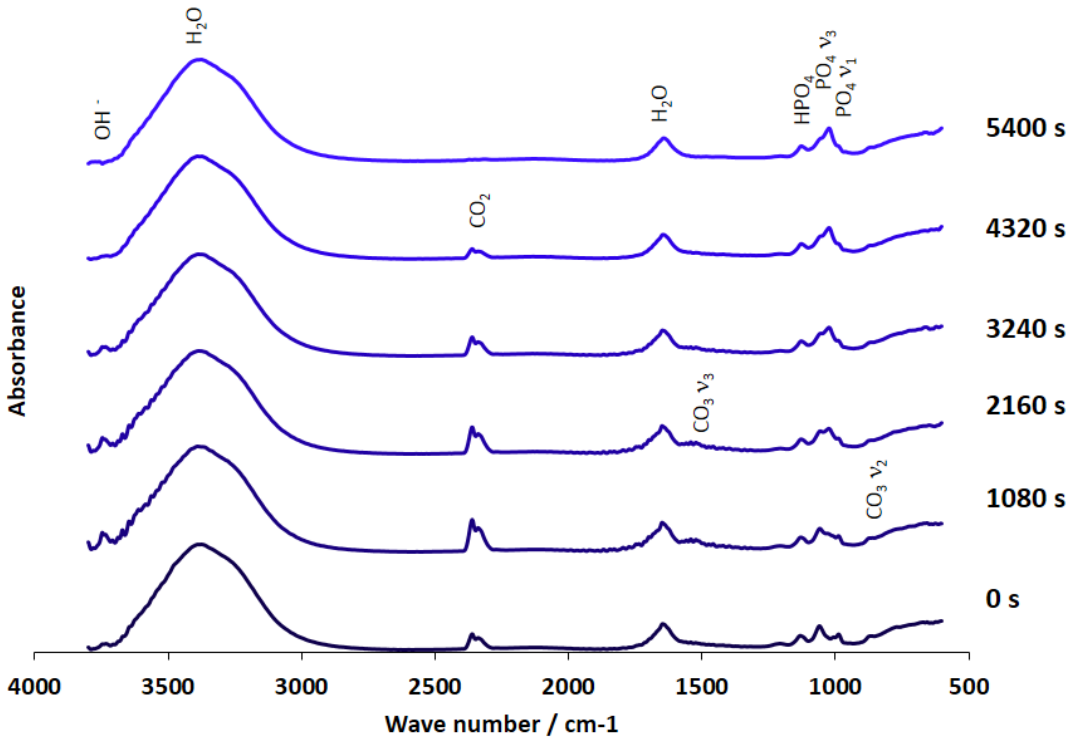

Fig. 2-2 Temporal profiles of FT-ATR-IR spectra of apatite cement in the course of the setting.

Fig. 2-2 shows the temporal change of corrected ATR-IR absorption spectra of the TeCP-DCPD mixture kneaded with phosphoric acid. The peaks in the range of 1500-1700 cm^{-1} and of 2800–3800 cm^{-1} are due to free water in aqueous phase. The spectra show characteristic peak shifts in the ranges of 2250–2400 cm^{-1} and 850–1050 cm^{-1}, attributable to the formation of HAp. As for the latter range, it is known that the absorption bands of HAp-related materials are respectively assigned to as follows [36-38]: the band at 3569 cm^{-1} to hydroxyl stretch; the bands at 962, 472, 976–1190 and 520–660 cm^{-1} to ν_1, ν_2, ν_3 and ν_4 vibrational modes of phosphate ions, respectively. At 5400 s after the kneading, the IR spectra of SSAC showed more characteristic peaks in the range of 850–1050 cm^{-1}, compared to at 0 s, due to ph. The CO_3 ν_3 broad peaks could faintly be seen in 1400–1550 cm^{-1} in this figure. It is known that CO_3 is contained in HAp products as an impurity. Such carbonated HAp is generally classified as A-type or B-type [39,40]. Carbonate ion is substituted with OH (Type A) or PO_4 (Type B) in HAp. Type A

carbonate gives doublet bands at about 1545 and 1450 cm^{-1} (asymmetric stretching vibration, ν_3) and 880 cm^{-1} (out-of-plane bending vibration, ν_2); Type B carbonate gives three bands at about 1455, 1410 and 875 cm^{-1} [41,42]. The CO_3 ν_2 peaks could be seen faintly at 871 cm^{-1} in this figure. This result suggests that B-type carbonate HAp is produced in the present study.

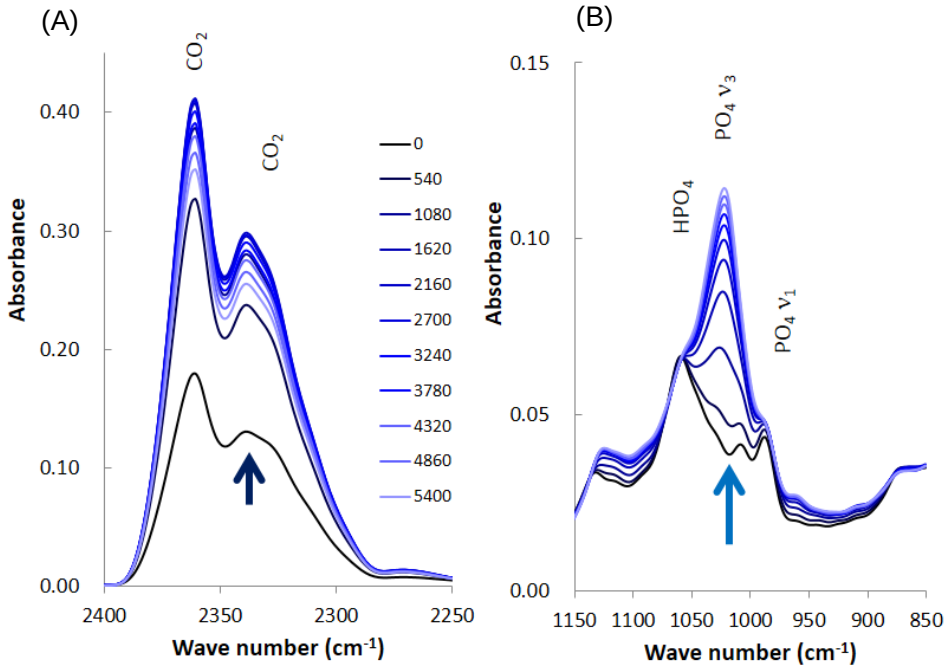

Fig. 2-3 The normalized ATR-IR spectra in the ranges of 850-1150 cm^{-1} (A) and 2250-2500 cm^{-1} (B).

Figs. 2-3 (A) and (B) shows the normalized ATR-IR spectra in the range of 2250–2400 cm^{-1} and 850-1150 cm^{-1}. The spectral change suggests that TeCP and DCPD in the raw cement have transformed into HAp by the kneading. That is, the absorption peak by phosphate group shifts from 1058 cm^{-1} (HPO_4) to 1024 cm^{-1} (PO_4), indicating the crystal transition to HAp from the raw cement [43]. The peaks at 2360 and 2340 cm^{-1} due to CO_2 did not shift but their intensities changed in a complex manner in the course of the formation of HAp. This result will be discussed in later section.

2.3.3 Principal component analysis

The normalized absorbance in the range of 850–1150 and 2250–2400 cm^{-1} (Fig. 2-3), which respectively correspond to CO_2 and phosphate group, are analyzed by PCA. Total residual variance for PCA, which was based on the change of ATR-IR spectra during the cement setting, were 4.14 and 1.20% for PC1 and PC2, respectively. Total explain value was 95.86 and 98.80% for PC1 and PC2, respectively.

It is important to control the number of principal component (PC) in multivariate analysis such as PCA, because unsuitable number of PC may cause unclear results. In order to clarify HAp formation, the effect of PC number of explain parameters should also be examined in detail. Ideally, simple models with minimal components, where the residual variance is ultimately zero, should be searched. The smaller total residual variance is, the more pieces of information in the variation can be explained. If this is not the case, it means that there are considerable noises in the data and/or that the data structure is too complex to be accounted for with a small number of components [32]. The residual variance of multivariate analysis of ATR-IR spectra has not only a quantitative analytical result but also qualitative chemical information about the products. As described in the previous section, the normalized ATR-IR spectra have information regarding to CO_2 in the suspension and phosphate group in HAp. Number of PCs for PCA needs, therefore, to be at least 2 so as to explain the change of ATR-IR

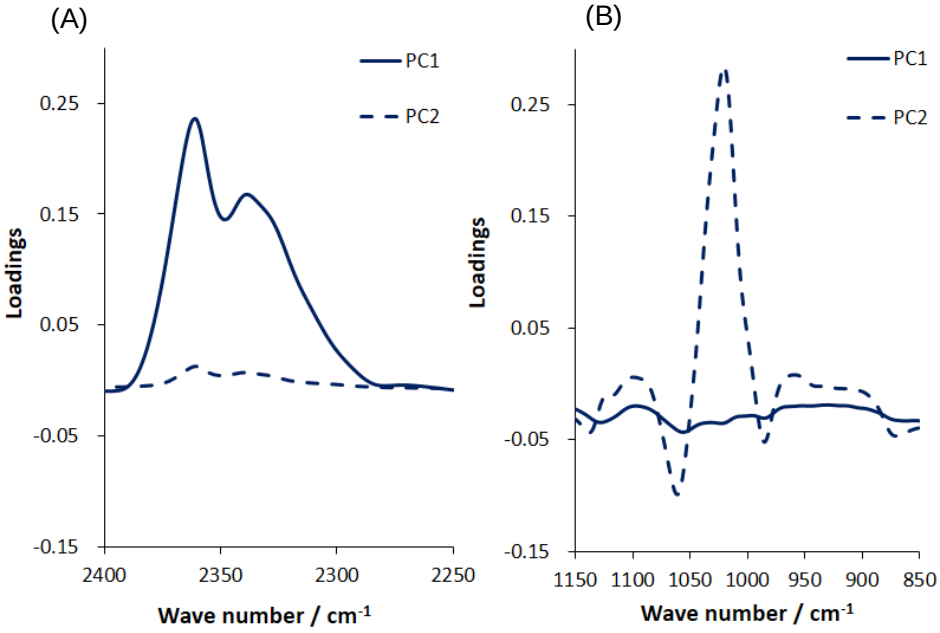

Fig. 2-4 Loading vectors PC1 and PC2 for PCA in the ranges of 850-1150 cm^{-1} (A) and 2250-2400 cm^{-1} (B).

spectra in the course of self-setting HAp formation.

Figs. 2-4 shows the loadings of PC1 and PC2 for PCA in the ranges of 850–1150 (A) and 2250–2500 cm^{-1} (B). PC1 have significant peaks in the range of 2250–2400 cm^{-1}, but does not have in the range of 850–1150 cm^{-1}. In contrast, PC2 have such peak in the range of 850–1150 cm^{-1}, but does not have in the range of 2250–2400 cm^{-1}. These results indicate that PC1 and PC2 are respectively correspond to CO_2 and phosphate group.

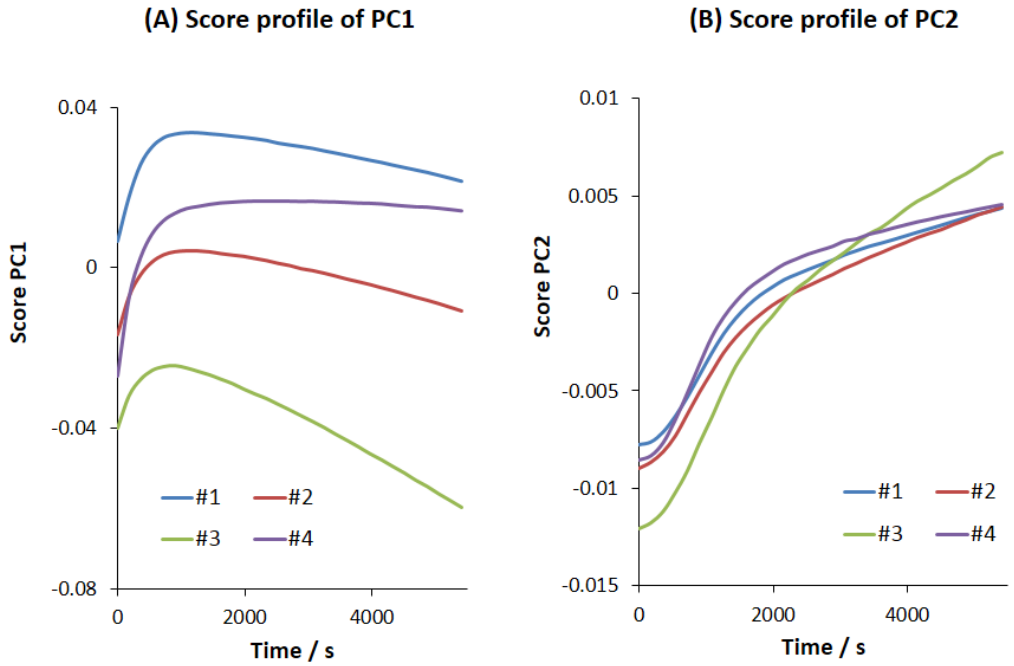

Fig. 2-5. Score profiles of PC1 (A) and PC2 (B) for the ATR-IR spectral data matrix of each SSAC setting process.

Figs. 2-5 (A) and (B), show the score profiles of PC1 and PC2 in the ATR-IR spectral data matrix of each SSAC sample as a function of setting time. Since the spectra are absorption profiles following Lambert Beer's law, the obtained scores of PC1 and PC2 correspond to the concentrations of CO_2 and phosphate group, respectively. The score profiles of PC1 (A) increased initially, reached to a maximum at around 1000 s, and then decreased. Although the variation of the scores is large between the samples, the tendencies are similar among them. In contrast, the score of PC2 (B) increased sigmoidally.

Fig. 2-6 shows the relationships between the scores of PC1 and PC2 for the samples. Initially, the change of PC1 is more significant than that of PC2. All profiles are similar in shape, but the variation in their values, especially in those of PC1, are very

large. The baseline shift in ATR-IR spectra, resulted from the differences in powder density, size distribution and background humidity are considered to attribute to the variation.

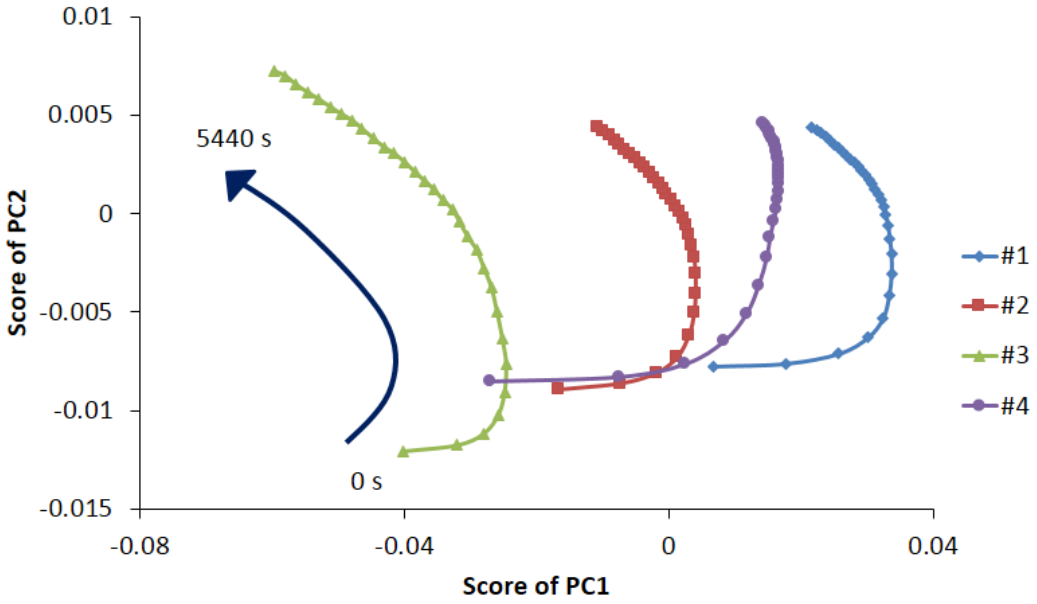

Fig. 2-6 Relationship between PC1 and PC2 scores for each SSAC setting process. Arrow indicates the time course of the process.

2.3.4 Principal component analysis with score time differentiate method

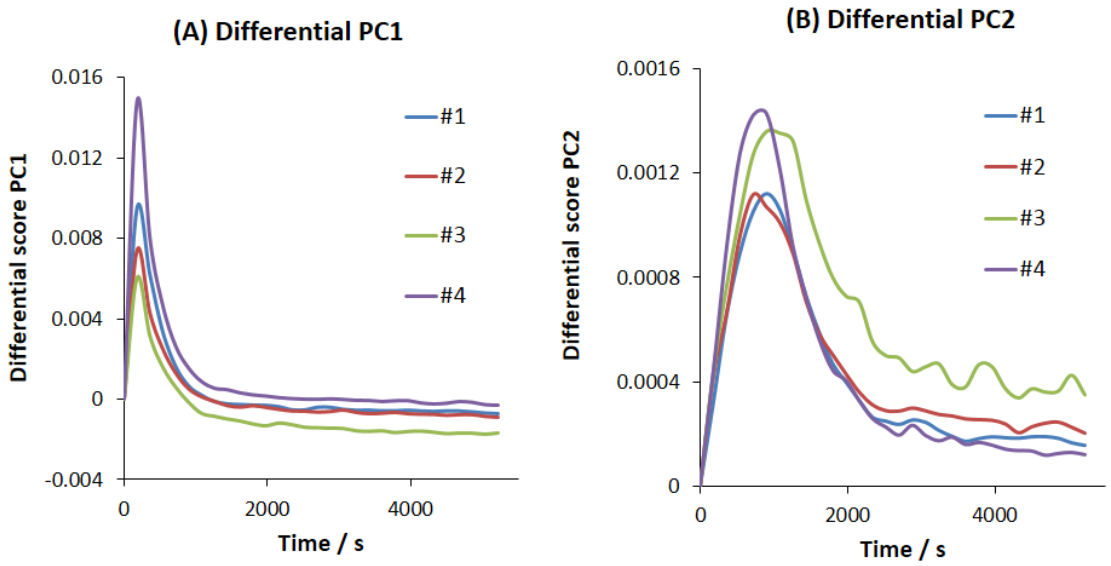

Fig. 2-7 Differentiated PC1 (A) and PC2 (B) score profiles for each SSAC phase transformation process.

In order to eliminate the variations among samples, the score were differentiated with respect to time. Figs. 2-7 (A), (B) show thus obtained differential scores of PC1 and PC2, respectively. The time differentiated PC1 scores increased initially with time, reached maxima at 180 s, and then decreased to zero at around 1000 s. After 2000 s, the scores become almost constant and have negative values. In contrast, the differentiated PC2 scores increased slowly, reached to maxima around 1000 s in contrast with 180 s for differentiated PC1, and then decreased.

Fig. 2-8 shows the relationship between differentiated scores of PC1 and PC2. It suggests that the transformation of SSAC consists of three major stages. In the first stage, the concentration change rate of CO_2 (corresponding to PC1) rapidly increases, and the recrystallization relating to phosphate group vibration (corresponding to PC2) starts. In the second stage, the concentration change rate of CO_2 decreases with time, but the crystallization rate still increases constantly. In the last stage, the concentration change rate of CO_2 slightly decreases to a negative value, and the HAp crystallization rate significantly decreases. From these results, CO_2 is considered to be not only the source of CO_3^{2-} of carbonated HAp but also a catalyst for HAp formation. Referring to

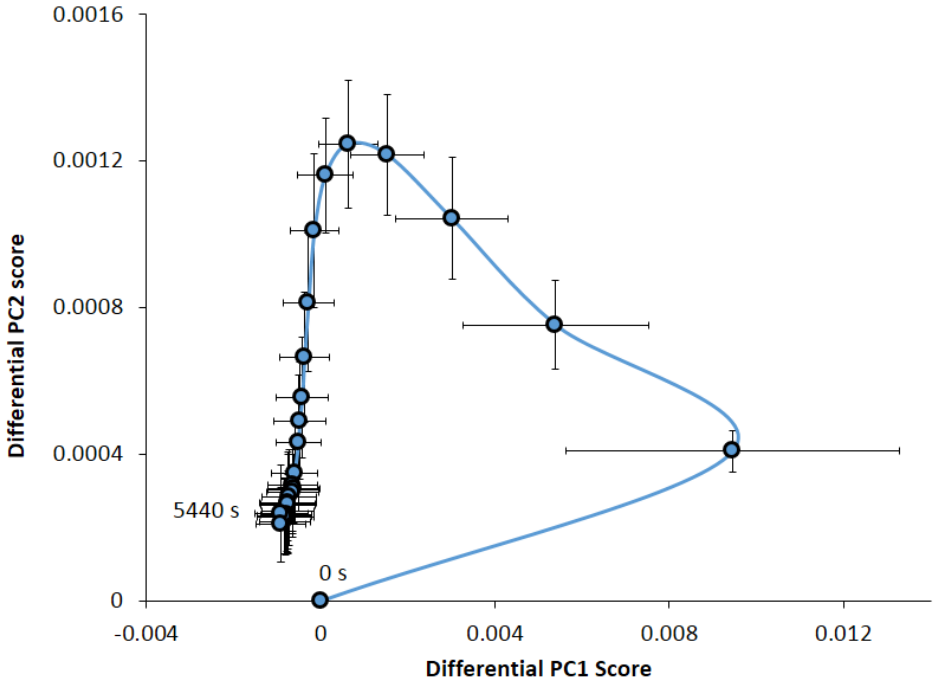

Fig. 2-8 Relationship between differentiated PC1 and PC2 scores for SSAC setting process. Horizontal and vertical bars indicate respective standard deviation (n = 4).

the report by Welch *et al.* [44], chemical reaction between the calcium phosphates and CO_2 is considered to be expressed as follows:

Henry's law indicates that the partial pressure of CO_2 gas is proportional to CO_2 concentration in suspension (Eqs. 2 and 3). CO_2 concentration in atmospheric air is constant at 381 ppmv (= 5.5 v/v%).

$$CO_2(g) \rightleftarrows CO_2(aq) \tag{2-2}$$

$$CO_2(aq) + H_2O(l) \rightleftarrows H_2CO_3(aq) \tag{2-3}$$

The hydration constant K_h for the reaction of Eq. 3 is 1.7×10^{-3} mol/L at 25°C.

$$CO_2(aq) + H_2O(l) \rightleftarrows H^+(aq) + HCO_3^-(aq), \quad pK_{a1}^* = 6.35 \tag{2-4}$$

$$K_{a1}^* = \frac{[H^+][HCO_3^-]}{[H_2CO_3] + [CO_2]} = 4.45 \times 10^{-7} \text{ mol/L} \tag{2-5}$$

where K^*_{a1} means the apparent first dissociation constant of carbonate acid, taking CO_2

concentration into accout.

$$HCO_3^-(aq) \rightleftarrows H^+(aq) + CO_3^{2-}(aq), \quad pK_{a2} = 10.33 \tag{2-6}$$

$$K_{a2} = \frac{[H^+][CO_3^{2-}]}{[HCO_3^-]} = 4.7 \times 10^{-11} \text{ mol/L} \tag{2-7}$$

CO_2 is ionized to CO_3^{2-} (Eqs. 2-3, 2-4, 2-6), the concentration of which is expressed in Eq. 7. The reactions of Eqs. 2−4 and 2-6 are reversible.

Fukase *et al.* [45] reported that the raw TeCP-DCPD cement transformed into stoichiometric HAp as follows:

$$2Ca_4(PO_4)_2O + 2CaHPO_4 \cdot 2H_2O \rightarrow Ca_{10}(PO_4)_6(OH)_2 + 4H_2O \tag{2-8}$$

Otsuka *et al.* [46] elucidated through their study employing FT-IR spectroscopy that an apatite cement transformed into carbonated HAp while absorbing a small amount of carbonate ion; carbonate ion in the carbonated HAp could be removed by laser irradiation. Hsu *et al.* reported that the chemical formulation of B-type carbonated HAp in mammalian bone was $[Ca_{10-x}Na_x(PO_4)_{6-x}(CO_3)_x(OH)_2]$ [36]. The present results indicate that the bulk powders of TeCP and DCPD irreversibly transformed into carbonated HAp in the presence of CO_2, after its being mixed with a kneading solution (Eq. 2-9).

$$2Ca_4(PO_4)_2O + 2CaHPO_4 \cdot 2H_2O + xH^+ + xCO_3^{2-} \rightarrow Ca_{10-x}(PO_4)_{6-x}(CO_3)_x(OH)_{2-x} + xCa^{2+} + xPO_4^{3-} + (4+x)H_2O \tag{2-9}$$

From Eq. 2-9, pH of the solution is considered to increase during the transformation. Doi *et al.* reported that the pH of the suspension changed from acidic to natural when TeCP and DCPD dissolved in 20 mM phosphoric acid at the powder/liquid ratio of 5 mL/g [47].

In the first stage of phase transition, CO_2 concentration (PC1) in the suspension increased (see Figs. 2-5 and 2-6). Both CO_2 in the solution and that on the solid surface contribute to the CO_2 concentration measured by ATR-IR. The CO_2 concentration in the solution is constant because the atmospheric CO_2 concentration is virtually invariable (Eq. 2-2). The present results suggest, therefore, the absorption/adsorption of CO_2 in/on the transformed solid from CO_2-rich super-saturated calcium phosphate solution, presumably, at the initial stage of transformation. In the second stage, the super-saturated solution formation still continued but some of them transformed to carbonated HAp while releasing excess CO_2. This release results in the decrease of differential score

of PC1 (Figs. 2-7 and 2-8). In the last stage, the reaction is approaching to the completion which means carbonated HAp formation, resulting in the negative differential score of PC1. The CO_2 acts, therefore, as a catalyst or mediator for the phase transition in addition to the source of carbonate ion in carbonated HAp. Although the final composition of the solid phase is not completely clear in the present study because the transformation was measured for 5400 s, some CO_2 molecules may be remained in the final product (carbonated HAp) without being converted to carbonate ion. Welch *et al.* reported such phenomena before [44]. Eidelman *et al.* measured the solubility of various types of calcium phosphates in the presence and absence of 5.5% CO_2 in the atmosphere. At 5.5% CO_2 concentration, undiluted ultrafiltered human serum was substantially under saturated, slightly supersaturated and highly supersaturated with respect to DCPD, OCP (octacalcium phosphate), and HAp, respectively [48,49]. These facts support the proposed mechanism that CO_2 affect the self-setting process of TeCP - DCPD apatite cement.

2.4 Conclusion

The HAp formation process from DCPD and TeCP suspension has been investigated by ATR-IR and chemoinformatics. The differentiated score is useful for understanding the complicated chemical reactions involved. The proposed approach is found useful for analyzing the rapid reaction such as the self-setting TeCP-DCPD apatite formation of the present study. The setting formation of SSAC consists of three stages, and CO_2 plays an important role for the transformation as a catalyst.

3. Effect of hydroxypropyl methylcellulose and hydroxypropyl cellulose on carbamazepine polymorphic transformation; attenuated total reflectance – infrared spectroscopy and chemoinfomatic analysis

3.1 Introduction

It is well known that many organic pharmaceutical compounds can exist in several polymorphic forms [9,51-55]. Polymorphic forms of active ingredient have great influence on physicochemical properties of pharmaceuticals such as crystalline density, transparency, specific surface area, hygroscopicity, solubility and chemical stability [56]. Especially, the transformation of an less soluble drug to a metastable polymorphic form influences the bioavailability of the pharmaceutical preparation through the increase of the dissolution rate [57]. As well as polymorphism, the degree of crystallinity has great influence on the physicochemical properties of pharmaceuticals. Combination of polymorphism and their degree of crystallinity can, therefore, control the quality of medications. In the previous study [9], the stability of theophylline anhydrate tablet has been studied under high humidity. Dissolution characteristics of the tablet is significantly suppressed in the humid condition due to the formation of theophylline hydrate, which has much lower solubility than the anhydrate. The technology to produce high-quality products from drugs including unstable polymorphs is one of the most essential issues in the pharmaceutical industry.

Fourier transform infrared (FT-IR) spectroscopy is one of the most versatile analytical methods that are used for the identification of materials and for the quantification of their components. FT-IR instruments can rapidly measure solid, liquid and gaseous materials with high sensitivity. The relationship between IR light absorption and the concentration of the component obeys Lambert-Beer's law. FT-IR spectroscopy can give chemical and physical information of materials that reflect vibrations (symmetrical/anti-symmetrical stretching, scissoring, *etc.*), light diffusivity and so on [58]. However, conventional FT-IR spectroscopy generally requires sample dilution with KBr powder because its sensitivity is too high to measure raw materials. In contrast, attenuated total reflectance (ATR), a technique for analytical signal sampling in IR spectroscopy, enables rapid and nondestructive measurement of as low as few mg of solid and liquid samples either in bulky or filmy state without any dilution.

Multivariate curve resolution (MCR) – Alternating least-squares (ALS) is a multivariate analysis that can be used for the analyses of reaction kinetics and of spectra data [59]. Himmelsbach and Holser applied MCR and 2D correlation to IR spectra in the

course of polymerization of glycerol and adipic acid [60].

In the prevent study, the molecular interaction between excipients and carbamazepine (CBZ) in wetted powder is investigated. An approach based on ATR-IR spectra and MCR is proposed as a tool of process analysis for the elucidation of the polymorphic transformation mechanism of CBZ.

3.2 Experimental

3.2.1 Materials

Carbamazepine anhydrate (CBZAH), hydroxypropyl cellulose (HPC) in SSL grade, and hydroxypropyl methylcellulose (HPMC) in CH-5-R grade were purchased from Wako Pure Chemical Industries, Nippon Soda and Shin-Etsu Chemical Industry Co., Japan, respectively. Aqueous solutions of 0.005 w/v% HPC and HPMC were prepared by respectively dissolving them in Milli-Q water.

3.2.2 Polymorphic transformation of CBZ

3.0 mg of CBZAH was kneaded with 35.0 μL of 0.005 w/v HPC or HPMC solution. The paste was put on a germanium glass of the ATR accessory and was covered with a sheet of Parafilm® at 20 ± 2 °C.

3.2.3 Powder X-ray diffraction analysis

Loosely packed sample was prepared in order to avoid crystal orientation when it was poured in the holder of the instrument without compression. The crystal phases in the specimens thus prepared were analyzed with a powder X-ray diffraction (XRD) system (Miniflex Rigaku Co. Ltd., Tokyo, Japan) at room temperature. Measurement conditions were as follows: Ni-filtered CuKα radiation (λ = 0.1540 nm); voltage, 30 kV; current, 15 mA; time constant, 1 s; step slit, 0.2°; counting time, 1.0 s; measurement range, 2θ = 5.0° ~ 45.0°.

3.2.4 ATR-IR spectroscopy

ATR-IR spectra were measured with an FTIR spectrometer (FTIR-6200, Jasco, Japan) equipped with a horizontal ATR plate (ATR PRO 610P-S, Jasco, Japan) with Germanium crystals. IR spectra of CBZAH paste suspended in the solutions were measured in the range of 2000-1000 cm^{-1} at a resolution of 8 cm^{-1} and acquired as digital data in a computer for further kinetic analysis. The spectrum for each sample was obtained through the averaging of the results of 74 scans, where the contribution from

the air was corrected as a background.

3.2.5 Generalized two-dimensional (2D) correlation spectroscopic analysis

Two-dimensional (2D) correlation spectroscopy, which was proposed by Noda *et al.* [61,62] has been applied to complicated spectral intensity variations of IR [63], Raman [64] and other optical signals having different waveforms. Advantages of the 2D analysis can be summarized as follows: (i) examination of spectra regardless of their phase; (ii) identification of various inter- and intramolecular interactions through selective correlation of bands; (iii) band assignments based on the correlations between various band positions.

An IR spectral intensity variation $A(\nu, T)$ observed in a compression pressure range of T_{min} - T_{max}, the synchronous and anti-synchronous 2D IR correlation intensities, $\phi(\nu_1, \nu_2)$, in the compression pressure range, is expressed by Eq. 3-1

$$\phi(\nu_1,\nu_2)+i\varphi(\nu_1,\nu_2)=\frac{1}{\pi(T_{max}-T_{min})}\int_0^\infty Y_1(\omega)Y_2^*(\omega)d\omega, \qquad (3\text{-}1)$$

where $Y_1(\omega)$ is the compression pressure-domain Fourier transform of $A(\nu_1, T)$, *and* $Y_2^*(\omega)$ is the conjugate of the Fourier transform of $A(\nu_2, T)$. Prior to the calculation of 2D correlation spectra, IR spectra were baseline-corrected. The equation for the baseline offset correction is as follows:

$$f(x)=x-\min(X), \qquad (3\text{-}2)$$

where $f(x)$ and $\min(X)$ are absorbance at χ cm^{-1} and minimum absorbance value of each spectra, respectively.

The 2D correlation spectra were obtained using a free software named 2D-shige (Ver 1.1) for Windows (developed by Morita, Kuwansei Gakuin University).

3.2.6 Software

The chemoinfomatics computations are performed by UNSCRAMBLER software version 10.2 64 bit (Camo Software AS, Oslo, Norway).

3.2.7 Multivariate curve resolution – Alternating least-squares analysis

The algorithm for MCR was reported in detail before [65-69]. MCR can decompose spectra of mixtures into the n pure contributions of respective components involved in the spectra. The baseline corrected IR spectra were arranged in a data matrix D ($r \times c$) with the spectral data in r rows and in c columns that are the absorbance at each wavelength.

The MCR decomposition of matrix D is carried out according to the following equation:

$$D_{(r,c)} = C_{(r,n)} S_{(n,c)}{}^{T} + E_{(r,c)} \qquad (3\text{-}3).$$

The matrix $C_{(r \times n)}$ is called concentration profiles, which describes the individual contributions of the n species involved in the given spectra. The matrix $S_{(n \times c)}{}^{T}$ is the spectral contribution of these n species in the c columns of the data matrix (pure spectra profiles). $E_{(r \times c)}$ is the residual matrix containing the data variance that cannot be explained by the product CS^{T}. One important and frequently used iterative approach to solve Eq. 3-3 is MCR - alternating least squares (MCR-ALS). The optimization process starts from the initial setting of C and S^{T}, which is then refined so as to yield profiles with chemical meaning. Critical aspects in the application of MCR-ALS are the determination of the number of factors or components that cause variability in the data set and the rotational ambiguity of the sample.

In the case of pure components having spectral responses, a common constraint is that only positive values are allowable for S^{T} and C. For a reaction where a reactant changes stoichiometrically to a product, the so-called equality constant can be applied under the restriction of mass balance, if chemical information about the spectra or concentration is available [70].

3.3 Results and Discussion

3.3.1 Characterization of CBZ hydration process by ATR-IR spectroscopy

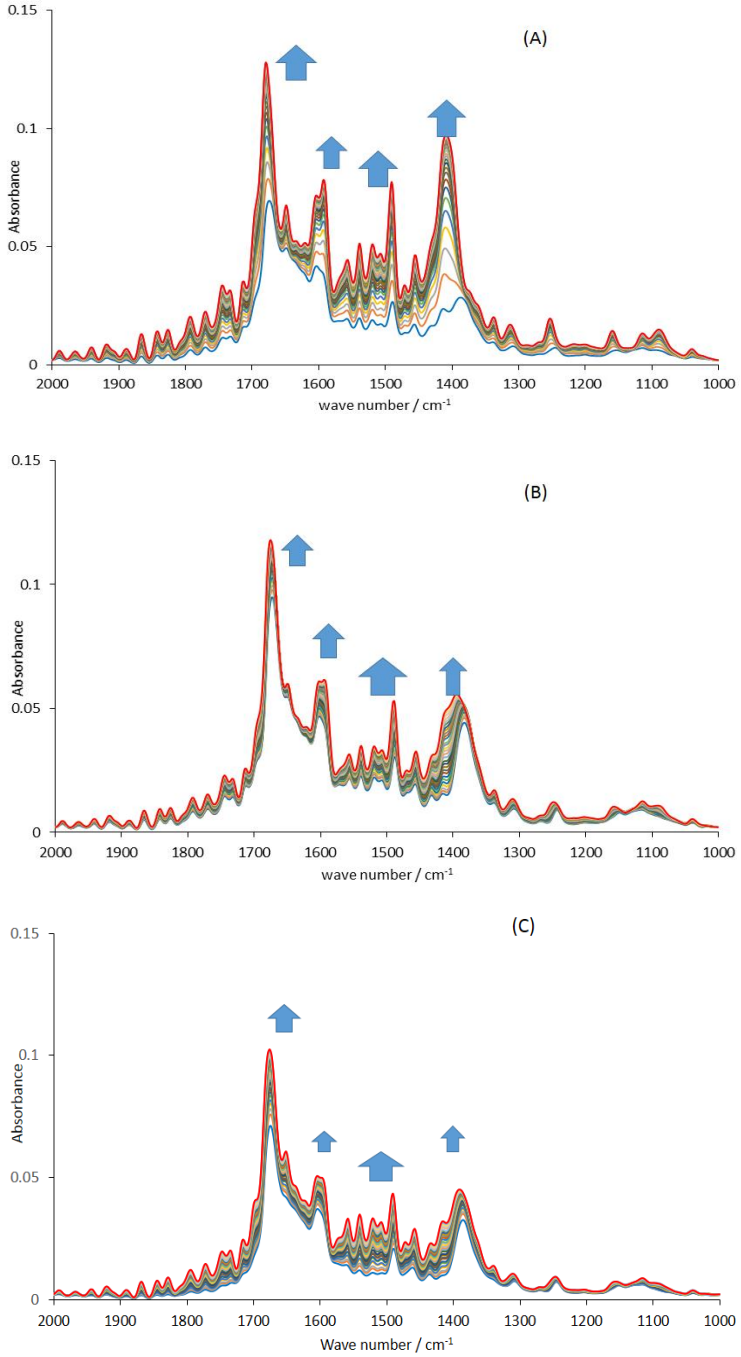

Fig. 3-1 Temporal profiles of ATR-IR spectra of CBZ powder kneaded with water (A), HPC (B) or HPMC (C) solutions.

Figs. 3-1 (A),(B) and (C) respectively show the changes of IR absorption spectra with time, where CBZ anhydrate (CBZAH) powder were kneaded with water (A) and aqueous solutions of HPC (B) and HPMC (C), respectively. These results indicate that CBZAH is transformed to CBZ dihydrate (CBZDH) by its being kneaded with the liquids. The peaks in IR spectrum of CBZ was reported as follows [71]: the peaks corresponding to symmetric stretching (ν_s) C=C in the dibenzazepine ring at 1488 cm^{-1}; the peaks corresponding to the ν_s C=O for associated and non-associated amide I at 1650 and 1690 cm^{-1}, where the peaks have red shift after the hydration [58]; the peaks assigned to the bending (σ) of NH_2 for associated and non-associated amide I at 1635 and 1605 cm^{-1}; the peak is assigned to the σ of OH for crystalline water at 1410 cm^{-1}.

3.3.2 Characterization of CBZ hydration process by PXRD

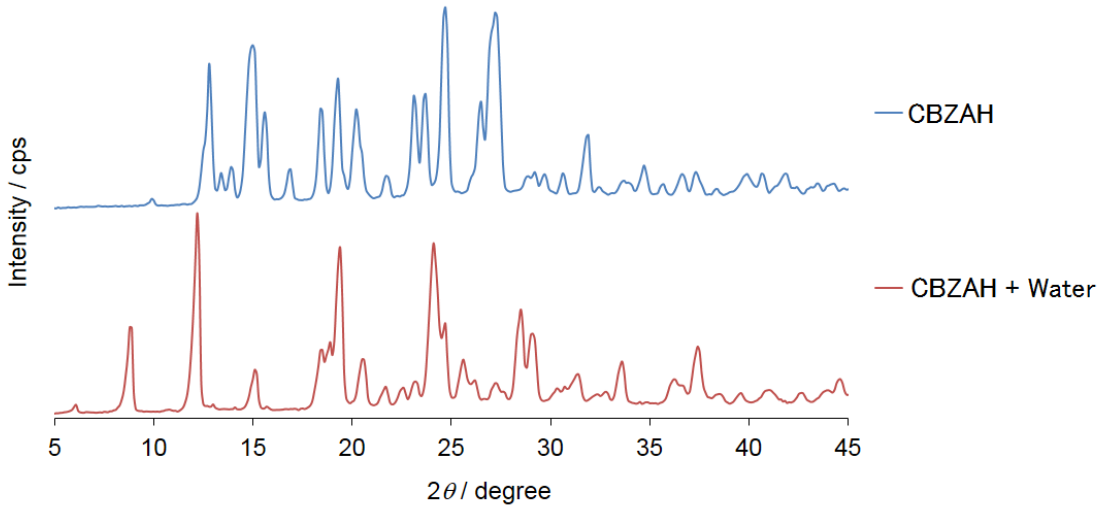

Fig. 3-2 PXRD pattern of CBZ AH and DH

Fig. 3-2 shows the powder X-ray diffractogram (PXRD) of CBZAH and that of CBZAH after its being kneaded with water for 1 day. The PXRD of CBZAH have distinct peaks at 12.8, 15.1, 15.6, 16.9, 18.5, 19.3, 20.3, 21.9, 23.1, 23.6, 24.7, 26.4, 27.3 and 31.8 °. The PXRD of the product after one day kneading had distinct peaks at 6.1, 8.9, 12.2, 15.2, 18.4, 19.1, 19.4, 20.4, 24.1, 25.6, 28.5, 28.6 and 29.1 °. The standard samples of CBZAH and CBZDH obtained according to the reference [72]. They respectively had the same PXRD profiles as those shown in Fig. 3-2. Suryanarayanan reported that the PXRD peaks at 12.8 and 8.9 ° are evidences for CBZAH and CBZDH, respectively, and the peaks intensity ratio could determine the quantity ratio of CBZAH

and CBZDH [72]. These PXRD results indicate that CBZAH transformed into CBZDH in the presence of water.

CBZAH were also kneaded with an aqueous solutions of HPC and HPMC for 1 day. The samples after the kneading were measured by PXRD. Both PXRD profiles obtained were identified as the profile of CBZDH. This result suggests that CBZAH transformed into CBZDH also in the presences of the polymer solutions. Harris *et al.* studied the structures of CBZAH and CBZDH [73]. The distance between the hydrogen bonded oxygen and nitrogen atoms varies over a range of 0.047 angstrom during the polymorphic transformation.

These results indicate that carboxyamide is the key group for the transformation from CBZAH into CBZDH. The polymorphic transformation is induced by the hydrogen bonding between the carboxyamide group and water in crystalline phase.

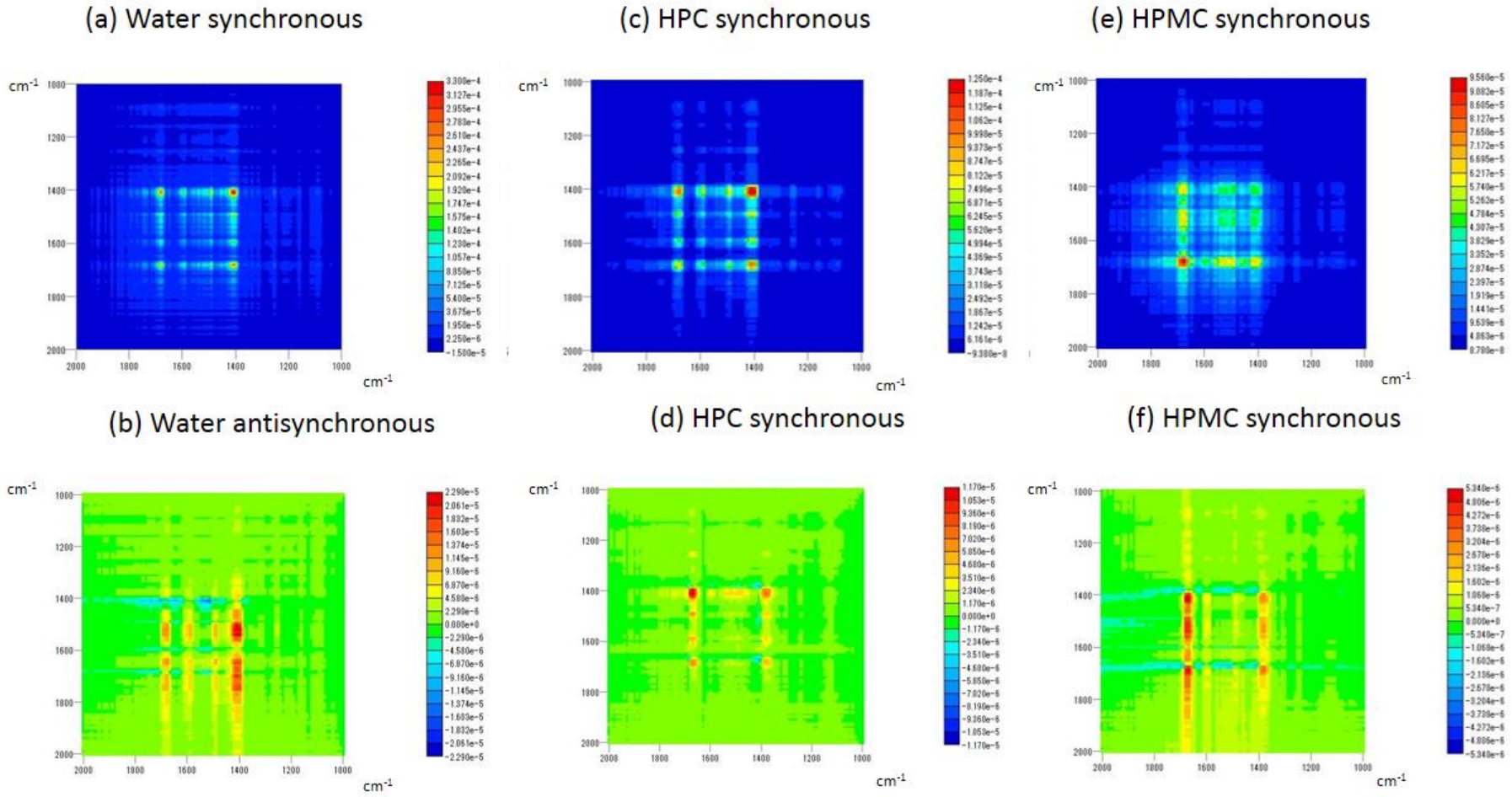

Fig. 3-3 2D correlation mappings of IR spectra change

3.3.3 Effect of polymer solution on 2D correlation analysis

Fig. 3-3 shows partial 2D correlation mappings calculated from the time-dependent IR absorption behaviors of CBZ shown in Fig. 3-1. Note that present partial 2D correlation analysis was carried out along the phase transformation time. As expected from the spectra of the CBZAH powder kneaded with water (Fig. 3-1 (a)), the emergence of a cross-peak at 1410 cm^{-1} and 1680 cm^{-1} were found in Fig. 3-3-(a), suggesting that changes in the OH σ and the C=O ν bands occur in the same directions. The partial synchronous 2D correlation mappings for CBZAH-HPC and CBZAH-HPMC systems (Figs. 3-3-(c) and -(e)) also show the apparent strong peaks at 1410 cm^{-1} and 1680 cm^{-1} corresponding to the OH σ and the C=O ν [74]. The 2D correlation spectra CBZ in the water and the HPC solution have the highest peak at 1410 cm^{-1} due to the OH σ, and the patterns are almost similar between them. The peak at 1410 cm^{-1} increased with the increase of that at 1680 cm^{-1}. In contrast, the 2D spectrum for CBZ in the HPMC solution (Fig. 3-3-(e)) has the highest peak at 1680 cm^{-1} due to the C=O ν, and the pattern is slightly different from those for the CBZ-water and CBZ-HPC systems.

Although the partial synchronous spectrum does not seem to provide direct information for understanding chemical interaction between CBZ and water, the 2D mapping can give valuable information about the hydration process through the combination with the corresponding anti-synchronous spectrum. The appearance of the anti-synchronous correlation peaks, in turn, indicates that there are two distinct populations, each having different band and unique molecular interaction between the functional groups of CBZ and water. It is noted that the partial anti-synchronous correlation spectra of CBZ hydration (Figs. 3-3-(b), (d) and (f)) show cross-peaks between 1400 and 1900 cm^{-1}. The discussion on the elucidation of cross-peaks in this region is especially important to clarify hydration mechanism. For example, if spectral intensities in this region simultaneously increase without any sequential or successive changes, only a synchronous correlation peak with no anti-synchronous correlation can be expected. The major positive cross peaks (Fig. 3-3 (b)) during the phase transformation of CBZAH in the presence of water were observed at 1490/1410, 1540/1410, 1550/1410, 1646/1410 and 1680/1410 cm^{-1}. The peak at 1410 cm^{-1} was due to hydrogen-bonded water. These results suggest that the transformation is triggered by the hydrogen bond formation of CBZ with water.

In contrast, the major cross peaks in the partial anti-synchronous spectrum of CBZ in the presence of HPMC (Fig. 3-3 (f)) were observed at 1409/1680, 1457/1680, 1595/1680, 1740/1680 and 1775/1680 cm^{-1}. The cross peaks associated with the C=O ν at 1680 cm^{-1} are more significant than the peaks associated with the OH σ at 1410 cm^{-1}.

This result suggests that the hydration is inhibited by HPMC absorbed on the surface of CBZ.

In the partial anti-synchronous spectrum of CBZ in the presence of HPC (Fig. 3-3 (d), the pattern of the major cross peaks was between those of CBZ-water and CBZ-HPMC systems. That is, the inhibitory effect on CBZ hydration by HPC was less significant than HPMC. Total residual variance for MCR-ALS, which was based on the change of ATR-IR spectra, were 9.75×10^{-6} and 2.06×10^{-6} for Source1 and Source2, respectively.

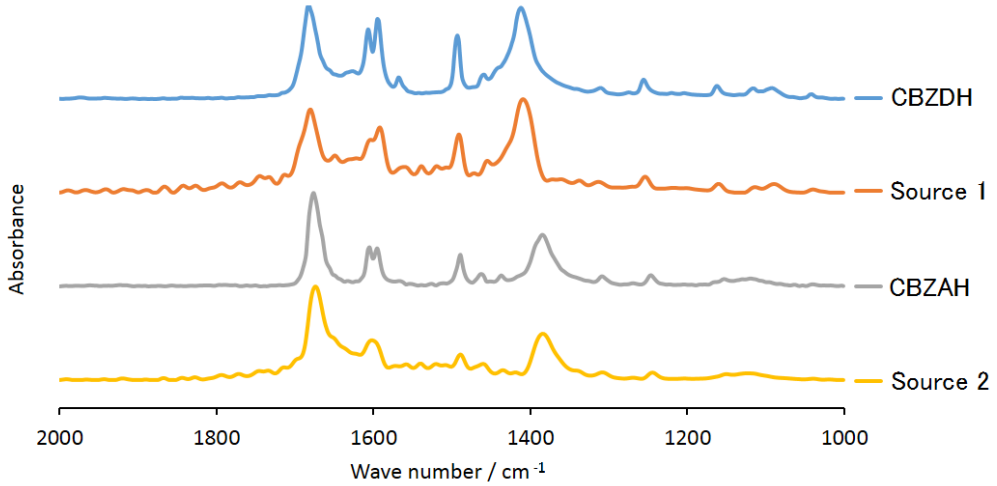

Fig. 3-4 Source and IR spectra of bulk materials.

3.3.4 Effect of polymer on hydration of CBZ; MCR-ALS analysis

IR spectra shown in Figs. 3-1 (A) - (C) were analyzed by MCR-ALS in order to evaluate the effect of polymer on hydration process. In the MCR-ALS computation, polymer amount in the solution is ignored because its concentration is sufficiently low enough to be ignored.

Source of the MCR-ALS and IR spectra of bulk CBZDH and AH are shown in Fig. 3-4. The Source 1 (S1) has significant peaks at 1128, 1154, 1248, 1314, 1340, 1386, 1464, 1488, 1604, 1673, 1700 and 1716 cm^{-1}. IR spectrum of bulk CBZDH has peaks at the same wavenumbers. In contrast, Source 2 (S2) has significant peaks at 1083, 1118, 1158, 1256, 1316, 1340, 1412, 1456, 1592, 1608, 1648, 1684, 1696 and 1718 cm^{-1}, all of which are contributed from CBZAH and water.

3.3.5 Kinetic studies of effect of polymer on hydration of CBZ; MCR-ALS analysis

Since IR spectra obey Lambert-Beer's law, the analytical results shown in Fig. 3-4 can be analyzed quantitatively. As mentioned, the source of the S1 aligns closely to the pure spectrum of CBZDH and, likewise, the source of S2 does so to CBZAH and water. Since each source factor can be assigned to a specific chemical component, it is possible to reveal changes of the components in carboxyl amide group of CBZ. Therefore, the concentration of CBZDH, C_{CBZDH}, is obtained by Eq. 3-4.

$$[C_{CBZDH}] = \frac{C_t^{S1} - C_0^{S1}}{C_{5440}^{Water\,S1} - C_0^{S1}} \tag{3-4}$$

Where C_t^{S1} , $C_0^{S1}$and $C_{5440}^{Water\,S1}$ are concentrations of Source 1 at the time of t, 0 and 5440 s, respectively, for the system of CBZAH and water.

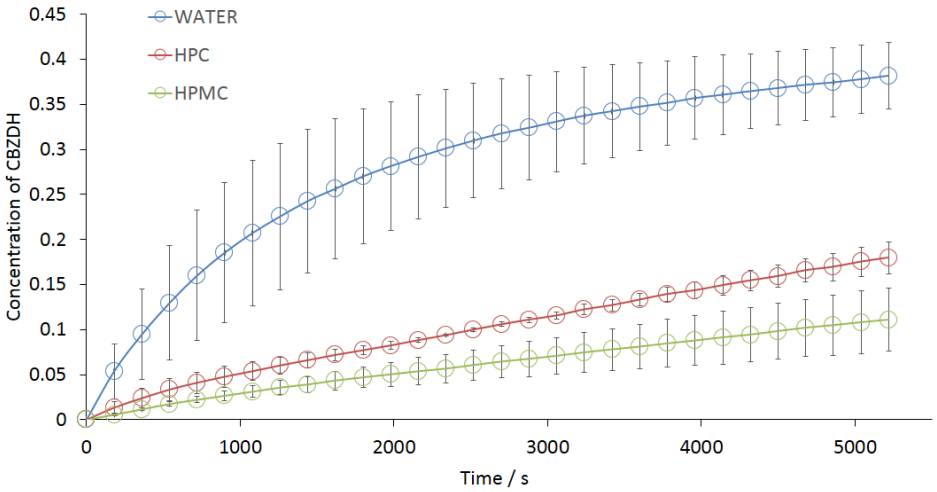

Fig. 3-5 Temporal profiles of CBZDH concentrations.

Fig. 3-5 shows the effects of the polymers on the profile of CBZDH concentration. In the CBZAH suspension in pure water, almost 100% of CBZAH was transformed into CBZDH at 5400 s. In contrast, in the suspensions in HPC and HPMC solutions, only 47.1% and 29.1% CBZAH, respectively, transformed into CBZDH at 5440 s. These results suggest that both polymer inhibit the polymorphic transformation.

Young and Suryanarayanan reported that CBZAH transformed into CBZDH in aqueous suspension in a first-order process [75]. In the present study, the polymorphic

transformation to CBZDH seems also to be followed by a first-order kinetics, where the transformation rate constant (k_{CBZDH}) is calculated from the least squares fitting curb as expressed by Eq. 3-5.

$$\frac{\partial -\ln(1-[C_{CBZDH}])}{\partial t} = k_{\mathrm{CBZDH}} \quad (0\ \% < [C_{CBZDH}] < 95\%) \qquad (3\text{-}5)$$

Where C^{S1}, $[C_{CBZDH}]$, t and k_{CBZDH} are the Concentration of S1 of MCR-ALS for IR spectra, corrected concentration (%) of CBZDH, time in seconds, and CBZDH concentration increase rate constant, respectively.

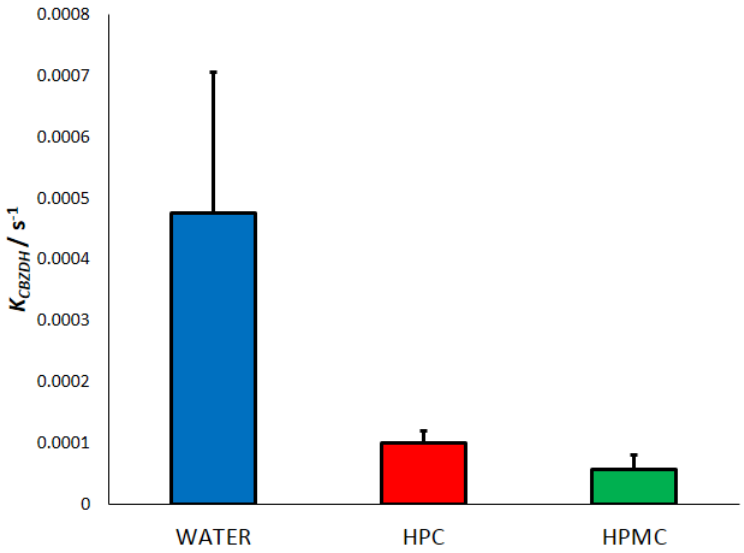

Fig. 3-6 Effects of polymers on k_{CBZDH}.

Fig. 3-6 shows the effects of polymers on k_{CBZDH}. The k_{CBZDH} in the water suspension (WATER) have the highest value and that in the HPMC suspension did so the lowest. The results of one-way analysis of variance of k_{CBZDH} are summarized in Table 3-1.

Table. 3-1 One-way analysis of variance of k_{CBZDH} of the prepared samples.

Solution	n	average	variant	Between solutions	
WATER	3	4.765×10^{-4}	5.326×10^{-8}	P value	F value
HPC	3	9.973×10^{-5}	4.157×10^{-10}	0.01617	5.143
HPMC	3	5.638×10^{-5}	5.314×10^{-10}		

Polymorphic transformation reaction from anhydrate into hydrate is reported to have three phases, as shown Fig. 3-7 [76].

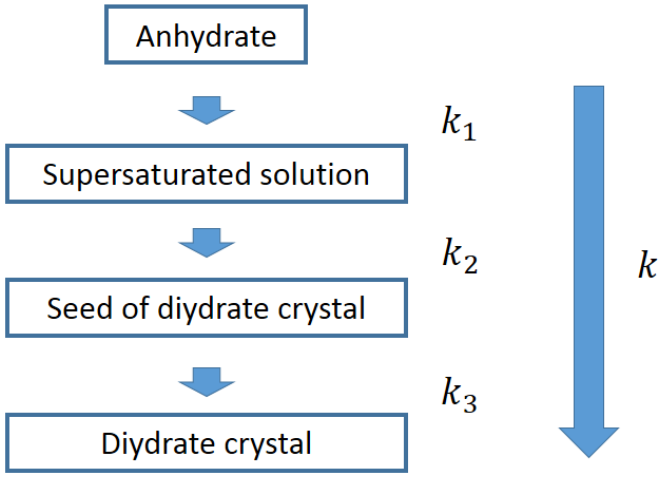

Fig. 3-7 Kinetics and elementary reaction of polymorphic transformation.

where k, k_1, k_2 and k_3 are apparent polymorphic transformation rate constant, dissolution rate constant, the nucleation rate constant and crystal growth rate constant, respectively. The symbol k is the overall transformation rate constant. It is known that the nucleation is generally rate-determining step. However, the profiles shown in Fig. 3-5 have no induction period. This fact indicates that the crystal growth step is the rate-determining step and that HPC and HPMC affect k_3.

3.4 Conclusion

CBZ polymorphic transformation in HPC and HPMC suspensions has been investigated by ATR-IR spectroscopy and chemoinfomatics (MCR-ALS). The combination of the two methodologies has been found useful for the elucidation of rapid polymorphic transformation in suspension. The polymorphic transformation rate is delayed by HPC and HPMC, supposedly through the decrease in the surface potential by the adsorbed polymer and that in diffusion coefficient due to the polymer in the solution.

4. Dry mechanochemical synthesis of caffeine / oxalic acid cocrystals and their evaluation by powder X-ray diffraction and chemometrics

4.1 Introduction

Solubility and dissolution rate of active pharmaceutical ingredient (API) are important factors for the development of pharmaceutical preparation [77-79]. In order to improve solubility characteristics, various basic approaches, such as cocrystallization, salt formation, complexation, encapsulation and so on, have been studied [80-83]. Vishweshwar *et al.* and Bathchelor *et al.* described that cocrystallization would gain a broader foothold in drug formulation [84,85]. Cocrystallization has attracted a lot of interest because of its potential for improving the physicochemical properties of drugs [86,87]. In general, pharmaceutical cocrystal consists of an active pharmaceutical ingredient (API) and coformer. There are many reports regarding the effect of cocrystallization on the physicochemical and pharmaceutical properties of API [88-91]. Moradiya *et al.* reported that carbamazepine (CBZ) dissolution rate was improved through its cocrystal formation with saccharin (SAC) [92]. Nehm *et al.* developed a mathematical model that describes the solubility of CBZ/nicotinamide cocrystal [93]. However they did not examined mechanochemical synthesis condition in detail.

A lot of cocrystallization methods, such as cocrystallization in supercritical fluid, slurry solution method, ultrasound-assisted crystallization and organic solvent evaporation method, have been studied for pharmaceutical preparation [94]. In cocrystallization process, the use of hazardous organic solvent is not desirable. Mechanochemical synthesis is a promising method because it does not need such organic solvent. The method is based on powder processing technique that involves deformation, fracturing and cold welding of particles in the course of repeating collisions under high energy milling [95]. Trask *et al.* applied the method to the preparation of caffeine (CA) / oxalic acid (OX) cocrystal [96]. The cocrystal was obtained within one hour from the mixture of CA anhydride and OX dihydrate at the molar ratio of 2:1.

Real time monitoring of cocrystallization in a non-contact and non-destruction mode is highly important for the manufacturing processes of pharmaceuticals. Conventionally, differential scanning calorimetry (DSC) [97] has been employed for the evaluation of the cocrystal formation. DSC is, however, a destructive method and needs a lot of time. In contrast, infrared (IR) and Raman spectroscopies are non-destructive

methods that can evaluate samples rather rapidly [98]. These method are, however, unable to analyze crystal structure, although they can identify functional groups in the crystals. In other hands, powder X-ray diffraction (PXRD) analysis is a powerful tool for the determination of the structure of crystals including cocrystals in a non-destructive fashion [99].

The Multivariate curve resolution - alternating least squares (MCR-ALS), one of chemometrics methods, can adopt various kinds of spectra data (*e.g.,* near IR, mid IR and ultraviolet-visible spectra) with overwrapped peaks. Maji *et al.* reported a quantitative analysis of strikarshika formulations by ultraviolet - visible spectroscopy coupled with MCR-ALS [100]. They decompose the spectra of microgynon and neogynona mixture samples into n pure contributions of respective components.

In a previous study, the author reported a predictive quantitative determination for contents of powders in multicomponent pharmaceutical formulations from complex PXRD profile [101]. The author studied polymorphic transformation kinetics of CBZ anhydrate by attenuated total reflection - infrared (ATR-IR) spectroscopy and MCR-ALS [102]; MCR-ALS was also proved to be useful to evaluate kinetics of crystalline transformation of pharmaceuticals.

In the present study, the author has further applied the combination of experimental and chemometrics approaches to elucidate the dry-mechanochemical conditions in detail. CA/OX system was selected for the present investigation. The effect of temperature, rotation speeds and grinding time of dry-mechanochemical synthesis on CA/OX cocrystal formation was elucidated by PXRD analysis and MCR-ALS.

4.2. Experimental

4.2.1 Materials

Caffeine anhydrate and oxalic acid dihydrate were purchased from Shizuoka Caffeine Co. Ltd. (Japan) and Wako Pure Chemical Industries Ltd. (Japan), respectively. They were stored at 298 K (25 ºC) under 30% relative humidity.

4.2.2 Methods

4.2.2.1 Sample preparation

The CA/OX 2:1 cocrystal samples were prepared by evaporate dry-mechanochemical or recrystallization synthesis. An automortal staler (MMPS-T1, AS ONE Co., Japan) was used for the former method, where the CA and OX were mixed at the molar ratio of 2:1 and grinded at 253 - 333 K for 0 - 180 min under the rotation speed of 400, 800 and 1200 rpm. The solvent used for the latter method was methanol - chloroform (1:1(v/v))[96].

4.2.2.2 Attenuated total reflection - Infrared spectroscopy

IR spectra of samples were measured with a Fourier transform (FT) -IR spectrometer (FT/IR-6200, JASCO Co., Japan) equipped with an attenuated total reflection (ATR) accessory. The ATR attachment was inserted directly in the light beam. The prepared sample powder was put on a germanium glass of the ATR accessory at room temperature. ATR-IR spectra of the suspensions were measured in the range of 2000 - 1000 cm-1 at a resolution of 2 cm-1. The spectra obtained were averaged and corrected for air background.

4.2.2.3 Thermal Analysis

DSC was performed with a DSC-8230 calorimeter (Rigaku Co. Ltd., Japan). The operating conditions in a open-pan system were as follows: 5.0 mg in sample weight, 10 K/min in heating rate, 310 - 610 K in heating range.

4.2.2.4 Powder X-ray Diffraction analysis

The prepared samples were analyzed with a PXRD diffractometer (Miniflex, Rigaku Co. Ltd., Japan) at room temperature. Measurement conditions were as follows : Ni-filtered Cu K□ radiation (λ¼ 0.1540 nm), voltage, 30 kV; current, 15 mA; time constant, 1 s; step slit, 0.2°; counting time, 1.0s; measurement range, 2θ = 5.0 - 30.0°.

The loosely packed powder was prepared by pouring the powder into the holder without high compression in order to avoid crystal orientation.

4.2.2.5 MCR-ALS method

The measured PXRD patterns were analyzed by MCR-ALS method for quantification. The residual can be eliminated from diffractogram data set for two component into account. MCR-ALS algorithm details have been reported elsewhere [103-107].

4.2.2.6 Software

The chemoinfomatics applications were performed by means of The Unscrambler® X version 10.3 (64 bit) from CAMO Software (Computer Aided Modelling, Trondheim, Norway).

4.3 Result and discussion

4.3.1 ATR-IR spectroscopy

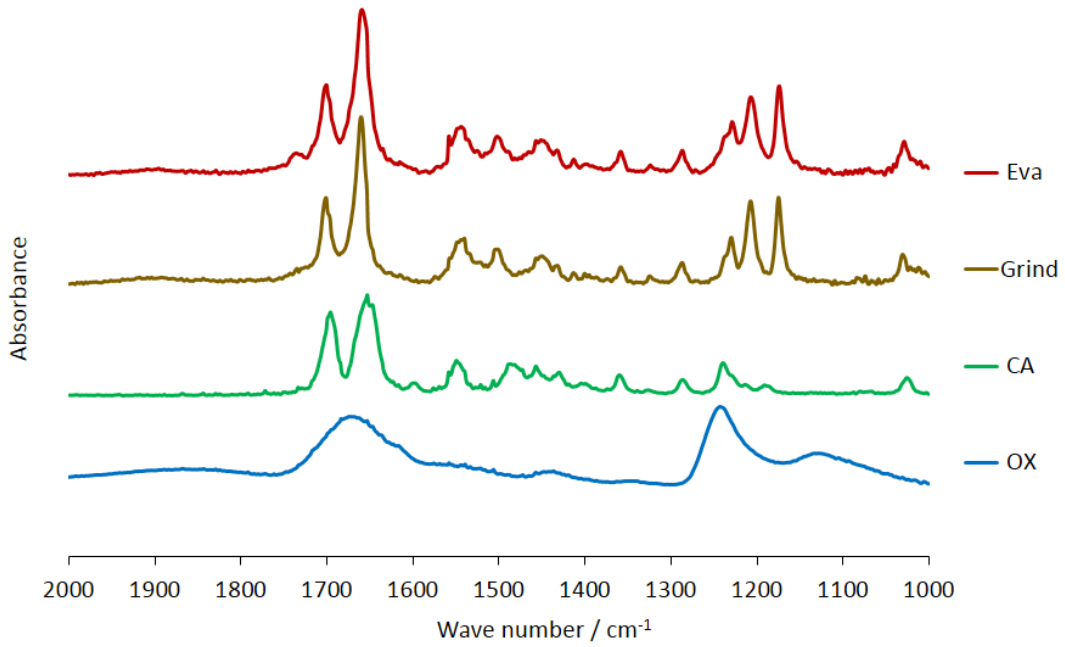

Fig. 4-1 ATR-IR spectra of the CA/OX cocrystals. The CA/OX cocrystal obtained by evaporation (Eva), physical mixing of CA and OX (Grind). ATR-IR spectra of CA and OX dihydrate bulk powders are shown.

Figure 4-1 shows ATR-IR spectra of the cocrystals synthesized by the evaporation method (Eva) and by the mechanochemical method (Grind), and those of CA and OX dihydrate crystals. The spectrum of CA has characteristic peaks at 1694, 1654, 1592, 1546, 1482, 1452, 1428, 1358, 1282, 1234 and 1018 cm^{-1}. That of OX dihydrate has at 1672, 1240 and 1126 cm^{-1}. On the other hand, Eva has the absorption peaks at 1732, 1698, 1658, 1544, 1500, 1446, 1352, 1320, 1286, 1232, 1208, 1172 and 1024 cm^{-1}. Grind has similar peaks to those of Eva, but no peak is observed at 1732 cm^{-1}. The peak at 1732 cm^{-1} is due to ν_{ring} of imidazole. The new IR peaks from cocrystallization appear at 1500, 1232, 1208 and 1172 cm^{-1}, which are respectively due to $\nu_{C=N}$, δ_{C-O-H}, ν_{C-O} and $\delta_{ring} + \rho_{CH3}$ [108]. Some studies have been carried out on IR spectra changes caused by cocrystallization [109-111]. In general, cocrystal formation of API and coformer is caused by the hydrogen bonding between them. Limwikrant *et al.* reported that the cocrystallization of CBZ and malonic acid induced the shift of IR peak for C=O stretching through hydrogen bonding [112]. Basavoju *et al.* showed the change of IR spectrum for

indomethacin/SAC cocrystal [113]. Gagniere *et al.* confirmed of solution-mediated phase transition of CBZ/nicotinamide cocrystal by means of ATR-IR spectroscopy [114]. Srinivasan *et al.* reported supra-molecular architecture constructed through the combination of strong and weak hydrogen bonds [115]. These ATR-IR spectroscopic results suggest that CA and OX effects on each other through the hydrogen bonding between them, resulting in IR spectra obtained in the present study. However, it is difficult to determine cocrystal concentration based on the ATR-IR peak shifts and their peak intensities. The author determine, therefore, cocrystal concentration based on PXRD analysis with MCR-ALS method.

4.3.2 DSC analysis

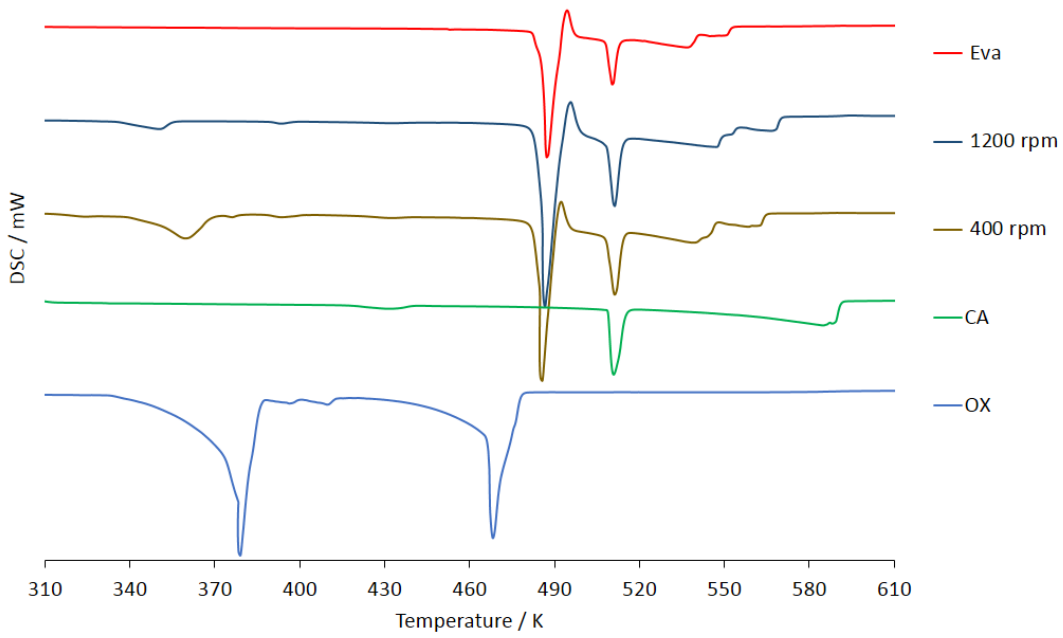

Fig. 4-2 DSC curves obtained for Eva and Grind. The grinding was carried out at 400 and 1200 rpm for 60 min at 310 K with 10 K/min. The DSC curves of CA and OX are also shown.

Figure 2 shows DSC curves of evaporated and grinded cocrystals (1200 rpm and 400 rpm) and of bulk powders of CA and OX. DSC curve of Eva (red curve) has the endothermic peaks at 487.7 and 510.8 K and exothermic peak at 493.3 K. The curve of cocrystal sample grinded at 1200 rpm (dark blue curve) has endothermic peaks at 350.9,

487.9, and 511.1 K and exothermic peak at 494.1 K. The curve of the cocrystal grinded at 400 rpm (yellow curve) has the endothermic peaks at 359.6, 487.9, and 511.4 K and exothermic peak at 491.4 K. In general, cocrystal products have exothermic peaks. These exothermic peaks are just the evidence for cocrystallization of CA and OX. The peaks at 431.2 and 510.8 K of CA bulk powder were respectively assigned to glass transition point and melting point, although the former peak seems not so clear.

Generally, dehydration peaks of hydrated appeared around at 373 K. The DSC results mentioned above suggest that the peaks at 350.9 and 359.6 K for 1200 and 400 rpm samples can be assigned to the dehydration point from unreacted OX dihydrate.
On the other hand, DSC curve of Eva has no peak in the range of 340-370 K. It was pointed out that CA/OX cocrystal is stable at high humidity and the crystal has no room to hold water molecular [96]. This result suggests that Eva has no bonding water, whereas grinded cocrystal samples contained OX dihydrate. Basavoju *et al.* observed in their study on DSC of indometachin/SAC that the melting point shifted during the cocrystallization [113]. Thermal behavior of indomethacin/SAC cocrystal was more distinct than that of each individual component. The DSC curve depends on the physicochemical properties of the samples. The present DSC result suggests that the change of physicochemical potential of cocrystal affects pharmaceutical properties.

4.3.3 PXRD analysis

Figure 3 shows the PXRD profiles for CA/OX cocrystal formation. Figure 3 (A) exhibits PXRD pattern of Eva, physically mixed powders of CA and OX dihydrate with no grind (denoted as “0 min” in Fig.3 (A)), CA anhydrate and OX dihydrate powders. Clear diffraction peaks of Eva are observed at 8.2, 12.0, 12.6, 16.4, 17.8, 18.8, 22.4, 24.6, 27.2, 28.4 and 28.8 degrees. Diffraction peaks of CA are at 11.8, 24.0, 26.2, 27.0 and 28.2 degrees; those of OX dihydrate are at 14.8, 18.8, 25.8 and 29.0 degrees. These results agreed well with those reported in the literatures [96,116,117]. The diffraction peaks of Eva at 8.2, 16.4, 17.8, 22.6, 24.4 and 27.2 degrees are reported to be due to CA/OX cocrystal structure [96]. Figure 3 (B) shows the effect of rotation speed of the auto mortar stirrer (1200, 800 and 400 rpm) on the diffractograms of the 2:1 CA/OX mixture samples grinded for 60 min. The characteristic peaks similar to those of Eva were observed after 60 min diffractogram. The peak at 11.8 degree is due to the (0, 1, 1) face of the cocrystal surface [96]. Figure 3 (C) shows the effect of grinding temperature (333, 310, 277, 253 K) on the PXRD profiles of the CA/OX mixture at the rotation speed of 1200 rpm and at the grinding time of 60 min. The diffractograms obtained are similar to that of Eva.

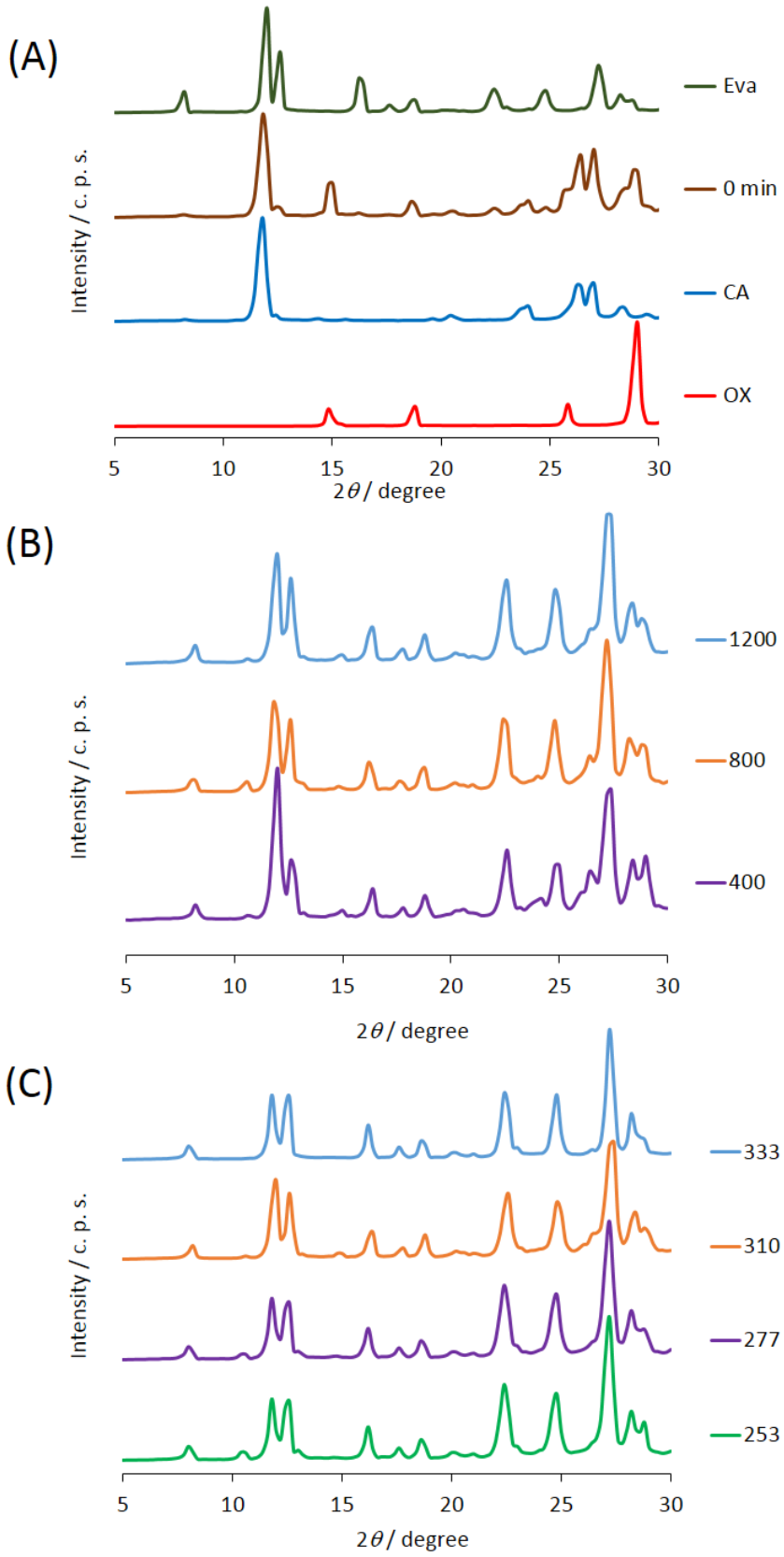
(A)
Eva
0 min
CA
OX
Intensity / c. p. s.
5
10
15
20
25
30
2θ / degree
(B)
1200
800
400
Intensity / c. p. s.
5
10
15
20
25
30
2θ / degree
(C)
333
310
277
253
Intensity / c. p. s.
5
10
15
20
25
30
2θ / degree

Fig. 4-3 (a) PXRD profiles of Eva, 0 min, CA, and OX, where “0 min” means the mixture of CA and OX before the grinding. (b) Effect of grinding rotation speed on PXRD profile of CA and OX mixture at the temperature of 310 K. (c) Effect of grinding temperature on PXRD profile of CA and OX mixture at the rotation speed of 1200 rpm.

4.3.4 MCR-ALS analysis

4.3.4.1 Source of MCR-ALS analysis

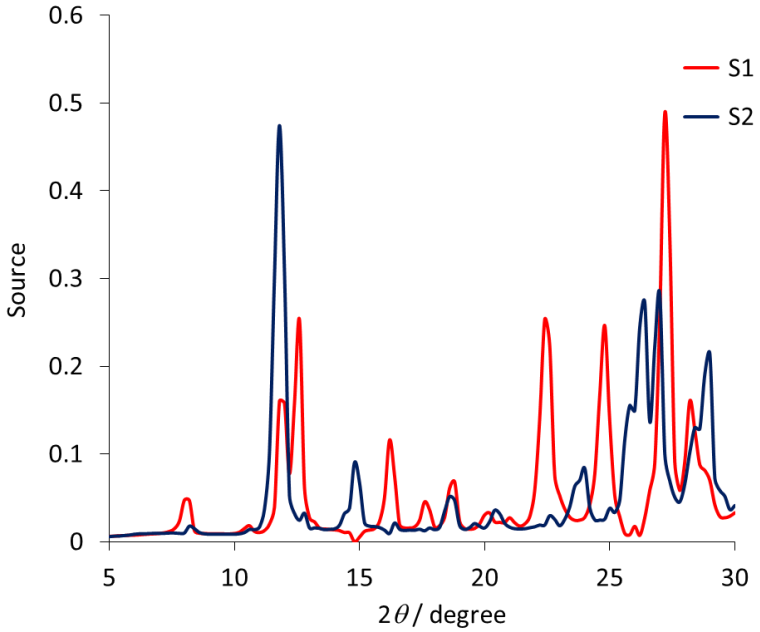

Fig. 4-4 Sources of MCR-ALS analysis based on the PXRD data set of the grinded produced samples.

Figure 4 shows the sources of MCR-ALS for the all PXRD profiles at two components. Produced cocrystal content of the grinded samples can be determined from results in this figure. The profiles of Source 1 (S1) and Source 2 (S2) have specific PXRD peaks due to CA/OX cocrystal and physical mixture of original compounds, respectively. Calvo *et al.* [118] evaluated cimetidine polymorphism from the R^2 value between source profile and IR spectrum. In order to compare of the similarity between each source profile and PXRD profile, R^2 values of respective profiles were calculated for peak intensities at

the diffraction angles of interest. Calculated R^2 values of S1 against PXRD profiles of the unreacted mixture of CA and OX mixture (0 min) and Eva were 0.501 and 0.109, respectively. On the other hand, the values of S2 against PXRD profile for the respective samples were 0.256 and 0.987. S1 and S2 of the $S^T_{(n\times c)}$ can, therefore, be assigned to the contents of unreacted CA and OX dihydrate mixture and the CA/OX cocrystal with $C_{(r\times n)}$, respectively. The R^2 value of S1 is, however, less than 0.7, meaning that the S1 is not completely the same profile as the PXRD profile of Eva. The result suggests that there are some differences in polymorphism or crystallinity between grinded cocrystal and organic evaporated cocrystal.

4.3.4.2 Effect of grinding time on the mechanochemical synthesis of cocrystal samples

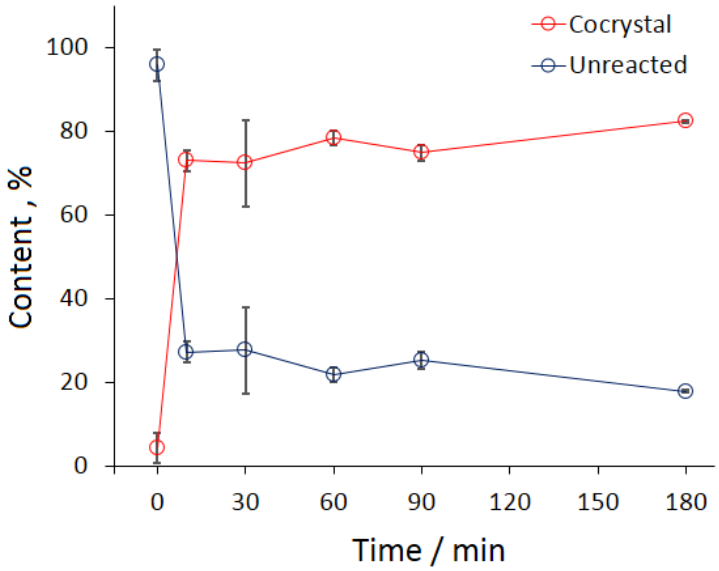

Fig. 4-5 The effect of grinding time on the contents of cocrystal and unreacted mixture at 1200 rpm and 310 K.

Figure 5 shows the effect of grinding time on the contents of cocrystal and unreacted mixture of CA and OX mixture. Before the grinding, CA/OX crystal content is 4 ± 3%. This result suggests that CA/OX cocrystal formation is not a spontaneous process and needs high activation energy. After the grinding at 1200 rpm for 10 and 30 min, the CA/OX cocrystal contents reached to 73 and 72 %, respectively. The effect of further grinding seems not so clear. Vangala *et al.* reported that the amorphous content of

CA/glutaric acid (1:1) cocrystal steeply increased to 65% within 15 min by a thermodynamic stability measurement [33]. Chieng *et al.* investigated on the kinetics CBZ/nicotinamide cocrystal formation in mechanochemical synthesis by a principal component analysis [119]. This result suggested final content of cocrystal is limited by the chemical equilibrium and after the equilibrium is reached, further grinding is not effective to increase the crystal content.

4.3.4.3 Effect of grinding temperature and rotation speed on the mechanochemical synthesis of cocrystal samples

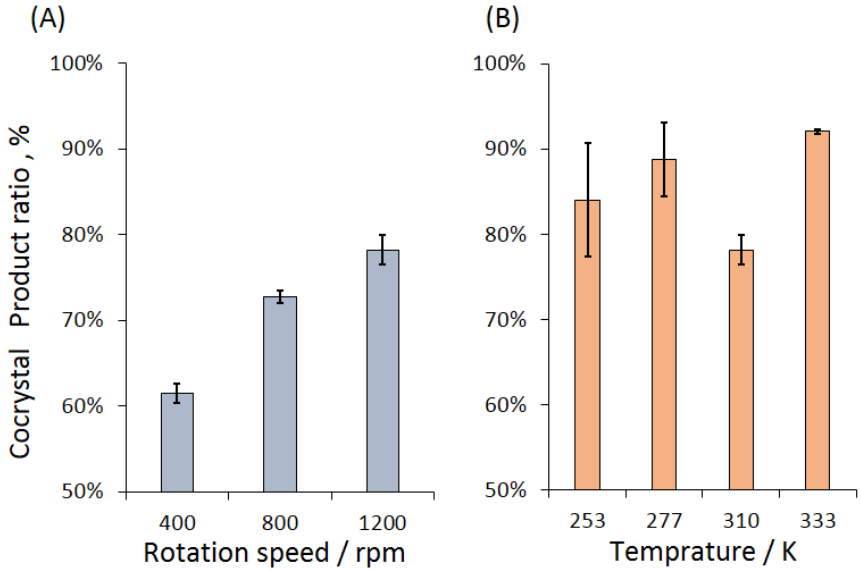

Fig. 4-6 The effect of grinding rotation speed (a) and temperature (b) on the produced cocrystal contents in the ground samples.

Figure 6 (A and B) show the effect of rotation speed at 310 K (A) and temperature at 1200 rpm (B) on the CA/OX cocrystal content produced by the mechanochemical synthesis. The time for the grind were kept at 1 hour for each sample. The contents were estimated by the MCR-ALS method. The contents at 400, 800 and 1200 rpm were 61 ± 1, 73 ± 1 and 78 ± 1%, respectively (Fig. 7 A). The contents at 253, 277, 310 and 333 K were 84 ± 7, 89 ± 4, 78 ± 1 and 92.1 ± 0.3%, respectively (Fig. 7 B). The effect of temperature was, however, not so significant within the range examined. The result suggests that the temperature is not critical factor to produce CA/OX cocrystal.

There are some reports describing the effect of milling energy on the

mechanochemical synthesis of the preparation of solid. Adzila *et al.* reported that rotation speed affect crystalline size and crystallinity of hydroxyapatite produced by a wet mechanochemical synthesis [120]. Fathi *et al.* reported the effect of rotation speed on the formation fluoridated hydroxyapatite nanoparticles [121]. Andrew *et al.* studied on the structures of five kinds of caffeine cocrystals with monocarboxylic acid, including formic, acetic and trifluoroacetic acids by PXRD [122]. In their study, different PXRD peaks appeared on the bulk CA profile. Chung *et al.* [123] investigated the effect of polymeric additives on the cocrystallization of caffeine by PXRD, IR spectroscopy, scanning electron microscopy and DSC. The poly(ethylene glycol) added disturbed the growth of cocrystals and decreased crystal size. They also discussed the dependence of characteristics of the powder samples on milling energy.

The 400 rpm rotated sample has more unreacted CA and OX dihydrate than the 1200 rpm rotated sample. DSC data (Fig. 2) of unreacted oxalic acid dehydrate, negative peak area in the range from 340 to 370 K due to water evaporation agreed well with unreacted OX dihydrate content obtained by MCR-ALS results. This agreement suggests that the combination of PXRD analysis and MCR-ALS approach is able to quantify the content of unreacted OX dehydrate. The method can decompose PXRD patterns into unreacted CA and OX mixed powders and CA/OX cocrystal. This combination would be applied widely to the developments of various cocrystallization development of drug seeds.

4.4 Conclusion

The effects of temperature, rotation speed and grinding time on dry-mechanochemical synthesis of CA/OX cocrystal have been studied based on PXRD patterns and MCR-ALS. The crystallinity of the produced cocrystal is different from that obtained by conventional evaporation method. The sources obtained by MCR-ALS are assigned to the produced cocrystal and the physical mixture of CA and OX dihydrate bulk powders.

Dry-mechanochemical cocrystal synthesis gives the chemical equilibrium at around 10 minutes after the grinding. The rotation speed is much more important than the temperature for the production of the cocrystal. Cocrystal contents are linearly increased with the speed. As far as we have surveyed, this is the first report on the PXRD analysis coupled with MCR-ALS for dry-mechanochemical cocrystal synthesis.

5. Acknowledgement

The author would like to express his sincere gratitude to Prof. Hideji Tanaka and Prof. Masaki Takeuchi, Lab. of Analytical Sciences, Graduate School of Pharmaceutical Sciences, Tokushima University for their constant guidance in the course of the work.

The authors would like to thank Prof. Besim Ben-Nissan (University of Technology, Sydney), Prof. David Grossin (University of Toulouse), Prof. Purnendu K. Dasgupta (University of Texas at Arlington), Prof. Kenichi Hamada and Dr. Ji-young Bae, (Tokushima University) for their help in interpreting the significance of the results of this study. The author is grateful to Mr. Akira Ito and Ms. Saki Matsumura Lab. of Analytical Sciences, Graduate school and Faculty of Pharmaceutical sciences, Tokushima University for their assistance in some of experiments.

This research was partly supported by Grant-in-Aid for JSPS Research Fellow Japan and Public-Private Partnership Student Study Abroad Program “TOBITATE! Young Ambassador Program”.

6. Reference

[1] S.D. Ross Inorganic infrared and raman spectra, (1972) McGraw-Hill, Maidenhead, UK.

[2] P. Larkin Infrared and raman spectroscopy; principles and spectral interpretation (2011) Elzevier, Nederland.

[3] M.I.Kay, R.A.Young, A.S. Posner. Crystal structure of hydroxyapatite. Nature (1964) 204: 1050-1502.

[4] K.Sunouchi, K. Tsuru, M. Maruta, G.Kawachi, S. Matsuya, Y. Terada, K. Ishikawa, Fabrication of solid and hollow carbonate apatite microspheres as bone substitutes using calcite microspheres as a precursor. Dent Mate J (2012) 31(4): 549–557.

[5] W.E. Brown, L.C. Chow, Dental restorative cement pastes, (1985) US. Patent No. 4518430A.

[6] C. Hamanishi, K. Kitamoto, A self-setting TTCP-DCPD apatite cement for release of vancomycin J Biomed Mater Res (1996) 33(3): 139-143.

[7] J.K. Haleblian, W. McCrone, Pharmaceutical Applications of Polymorphism, J Pharm Sci (1969) 58: 911.

[8] ICH harmonized guideline. Q6A Specifications, Test Procedures and Acceptance Criteria for New Drug Substances and New Drug Products, Chemical Substance, (1999).

[9] Y. Otsuka, M. Yamamoto, H. Abe, M. Otsuka, Effects of polymorphic transformation on pharmaceutical properties of direct compressed tablets containing theophylline anhydrate bulk powder under high humidity, Collo Surf B (2013) 102: 931– 936.

[10] S. Byrn, R. Pfeiffer, M. Ganey, C. Hoiberg, G. Poochikian. Pharmaceutical solids: A strategic approach to regulatory considerations, Pharm Res (1995) 12: 945.

[11] B. Shah, V.K. Kakumanu, A.K. Bansal, Analytical techniques for quantification of amorphous crystalline phases in pharmaceutical solids. J Pharm Sci (2006) 95: 1641.

[12] H. Martens, T. Naes, Multivariate Calibration. John Wiley Sons Ltd, Chichester, UK. (1989)

[13] W. Windig, C.E. Heckler, F.A. Agblevor, R.J. Evans, Chemometr Intell Lab (1992) 14: 195.

[14] N.L. Calvo, R.M. Maggio, T.S. Kaufman, A dynamic thermal ATR-FTIR/chemometric approach to the analysis of polymorphic interconversions. Cimetidine as a model drug J Pharmaceut Biomed (2014) 92, 90–97.

[15] Guidance for Industry PAT, Food and drug administration, http://www.fda.gov/.

[16] J. Luypaert, D.L. Massart, H.Y. Vander, Near-infrared spectroscopy applications in

pharmaceutical analysis. Talanta (2007) 72(3): 865–883.

[17] T.R.M. De Beer, P. Vercruysse, In-line and real-time process monitoring of a freeze drying process using Raman and NIR spectroscopy as complementary process analytical technology (PAT) tools. J Pharm Sci (2009) 98(9): 3430-3446.

[18] M. Andersson, S. Folestad, Quantitative analysis of film coating in a fluidized bed process by in-line NIR spectrometry and multivariate batch calibration. Anal Chem (2001) 72(9): 2099-2108.

[19] H.W. Denissen, K. de Groot, Tissue response to dense apatite implants in rats. J Biomed Mater Res (1980) 14(6): 589-597.

[20] Y.C. Hong, J.T. Wang, The periapical tissue reactions to a calcium phosphate cement in the teeth of monkeys J Biomed Mater Res (1991) 25(4): 485–498.

[21] B.R. Constantz, I.C. Ison, Skeletal repair by in situ formation of the mineral phase of bone. Science (1995) 267(5205): 1796-1799.

[22] H. Hamada, H. Ohshima, M. Otsuka, Dissolution medium responsive simvastatin release from biodegradable apatite cements and the therapeutic effect in osteoporosis rats. J Appl Biomater Funct Mater (2012) 10(1): 22-28.

[23] Y. Miyamoto, K. Ishikawa, In vivo setting behavior of fast-setting calcium phosphate cement' Biomaterials (1995) 16(11): 855-860.

[24] I. Petrov, B. Šoptrajanov, Infra-red investigation of dicalcium phosphates. Spectro Acta A (1967) 23(10): 2636-2646.

[25] M.C. Chang, J. Tanaka, FT-IR study for hydroxyapatite/collagen nanocomposite cross-linked by glutaraldehyde. Biomaterials (2002) 23(24): 4811–4818.

[26] T.K. Ronson, A.J. McQuillan, Infrared Spectroscopic Study of Calcium and Phosphate Ion Coadsorption and of Brushite Crystallization on TiO_2. Langmuir (2002) 18(12): 5019-5022.

[27] G. Ulian, G. Valdre, M. Corno, P. Ugliengo, The vibrational features of hydroxylapatite and type A carbonated apatite: A first principle contribution. Amer Mineral (2013) 98(4): 752-759.

[28] T. Næs, T. Isaksson, T. Fearn, T. Davies, A User-Friendly Guide to Multivariate Calibration and Classification, NIR publications: Chichester, (2002).

[29] H. Martens, T. Næs, Multivariate Calibration, John Wiley & Sons: Chichester (1989).

[30] F.G. Halaka, G.T. Babcock, and J.L. Dye, The use of principal component analysis to resolve the spectra and kinetics of cytochrome c oxidase reduction by 5,10-dihydro-5-methyl phenazine. Biophys J (1985) 8(2): 209–219.

[31] Y. Otsuka, M. Yamamoto, H. Abe, M. Otsuka, Effects of polymorphic transformation on pharmaceutical properties of direct compressed tablets containing theophylline

anhydrate bulk powder under high humidity, Colloid Surf B 102 (2013) 931-936.

[32] CAMO Software Research & Development Team "Welcome to The Unscrambler® X" http://support.camo.com

[33] H. Shinzawa, K. Awa, W. Kanematsu, Y. Ozaki, Multivariate data analysis for Raman spectroscopic imaging. J Raman Spec (2009) 40(12): 1720–1725.

[34] S. Hayakawa, T. Kanaya, Heterogeneous structure and in vitro degradation behavior of wet-chemically derived nanocrystalline silicon-containing hydroxyapatite particles. Acta Biomaterialia (2013) 9(1): 4856–4867.

[35] M. Otsuka, Y. Matsuda, Effect of particle size of metastable calcium phosphates on mechanical strength of a novel self-setting bioactive calcium phosphate cement. J Biomed Mater Res (1995) 29(1): 25-32.

[36] J. Hsu, J.L. Fox, Metastable Equilibrium Solubility Behavior of Carbonated Apatites .J Colloid Interface Sci (1994) 167(2): 414-423.

[37] I. Rehman, W. Bonefield, Characterization of hydroxyapatite and carbonated apatite by photo acoustic FTIR spectroscopy. J Materials Medicine (1997) 8(1) 1-4.

[38] R.Z. LeGeros, Calcium Phosphates in Oral Biology and Medicine. Monographs in Oral Sciences. (1991) 15. Myers HM (ed). Karger: Basel.

[39] R.Z. Legeros, O.R. Trautz, J.P. Legeros, E. Klein, W.P. Shirra, Apatite crystallites: effects of carbonate on morphology. Science (1967) 155(3768): 1409-1411.

[40] L. Müller, E. Conforto, D. Caillard, M.A. Frank, Biomolecular Engineering (2007) 24(5): 462-466.

[41] M. Otsuka, K. Papangkorn, A.A. Baig, W.I. Higuchi, Chemometric evaluation of physicochemical properties of carbonated-apatitic preparations by Fourier transform infrared spectroscopy. J Biomed Mater Res A (2012) 100(8): 2186–2193.

[42] J.C. Elliott, D.W. Holcomb, R.A. Young, Infrared determination of the degree of substitution of hydroxyl by carbonate ions in human dental enamel. Calcified Tissue Inter (1985) 37(4): 372-375.

[43] M. Otsuka, Y. Matsuda, Z. Wang, J. L. Fox and W. I. Higuchi, Effect of Sodium Bicarbonate Amount on In vitro Indomethacin Release from Self-Setting Carbonated-Apatite Cement Pharm Res (1997) 14 (4): 444-449.

[44] J.W. Michael, J.F. Lifton, J.A. Seck, Tracer studies with radioactive oxygen-15. Exchange between carbon dioxide and water. J Phys Chem (1969) 73(10): 3351–3356.

[45] Y. Fukase, E.D. Eanes, S. Takagi, L.C. Chow, W.E. Brown, Setting Reactions and Compressive Strength of Calcium Phosphate Cements, J Dent Res (1990) 69: 1852-1856.

[46] M. Otsuka, Y. Matsuda, Effect of CO_2 Laser Irradiation on Surface Hardness of Self-

Setting Hydroxyapatite Cement, Chem Pharm Bull (1991) 39(10): 2753 – 2755.

[47] Y. Doi, S. Shibata, Y. Takezawa, N. Wakamatsu, H. Kamemizu, M. Iijima, Y. Moriwaki, U. Katsumi, F. Kubo, Y. Haeuchi, Self-setting Apatite Cement : III, Setting Mechanism, Jpn Soc Dental Mat Dev (1988) 7(2): 176-183.

[48] N. Eidelman, L.C. Chow, W.E. Brown, Calcium Phosphate Saturation Levels in Ultrafiltered Serum. Calcif Tissue Int (1987) 40(2): 71-78.

[49] N. Eidelman, L.C. Chow, W.E. Brown, Calcium phosphate phase transformations in serum. Calcif Tissue Int (1987) 41(1): 18-26.

[50] J. Luypaert, D.L. Massart, Y. Vander Heyden, Near-infrared spectroscopy applications in pharmaceutical analysis. Talanta (2007) 72(3): 865–883.

[51] S.R. Byrn., Solid State Chemistry of Drugs, Academic Press, New York, (1982).

[52] G.A. Stephenson, J.G. Stowell, Solid-state investigations of erythromycin a dihydrate: Structure, NMR spectroscopy, and hygroscopicity J Pharm Sci (1987) 86 (11): 1239–1244.

[53] E.B. Vadas, P. Toma, G. Zografi, Solid-State Phase Transitions Initiated by Water Vapor Sorption of Crystalline L-660,711, a Leukotriene D4 Receptor Antagonist. Pharm Res (1991) 8(2): 148–155.

[54] M.J. Kontny and G. Zografi, Moisture sorption kinetics for water-soluble substances IV: Studies with mixtures of solids. J Pharm Sci (1985) 74(2): 124–127.

[55] V. Campen, G.L. Amidon, G. Zografi, Moisture sorption kinetics for water-soluble substances II: Experimental verification of heat transport control J Pharm Sci (1983) 72(12): 1388–1393.

[56] J. D Kirscha and J. K Drennenb, Nondestructive tablet hardness testing by near-infrared spectroscopy: a new and robust spectral best-fit algorithm. J. of Pharm. and Biomed Ana (1999) 19(3–4): 351–362.

[57] Y. Kobayashi, S. Ito, S. Itai, K. Yamamoto, Physicochemical properties and bioavailability of carbamazepine polymorphs and dihydrate. Int J Pharma (2000) 193(2) 137–146.

[58] N.B. Colthup, L.H. Daly, S.E. Wiberley, Introduction to Infrared and Raman Spectroscopy, Academic Press, New York, (1990).

[59] T. Azzouz, R. Tauler, Application of multivariate curve resolution alternating least squares (MCR-ALS) to the quantitative analysis of pharmaceutical and agricultural samples. Talanta (2008) 74(5): 1201-1210.

[60] D. Himmelsbach, R. A. Holser, Application of 2D correlation spectroscopy with MCR in the preparation of glycerol polyesters. Vib Spectro (2009) 51(2):142–145.

[61] I. Noda, A.E. Dowrey, C.S. Marcott, Y. Ozaki, Generated two-dimensional correlation

spectroscopy, Appl Spectrosc (2000) 54: 236A.

[62] I. Noda, Determination of two-dimensional correlation spectra using the Hibert transform. Appl Spectrosc (2000) 54: 994.

[63] M. Muler, R. Buchet, U.P. Fringeli, J Phys Chem (1996) 100: 10810.

[64] I. Noda, Y. Liu, Y. Ozaki, Two-dimensional correlation spectroscopy study. J Phys Chem (1996) 100: 8674.

[65] R. Tauler, Smilde, A. Kowalski, B. Selectivity, local rank, 3-way data-analysis and ambiguity in multivariate curve resolution. J Chemom (1995) 9: 31–58.

[66] R. Tauler, Multivariate curve resolution applied to second order data. Chemom Intell Lab Syst (1995) 30, 133–146.

[67] A. De Juan, R. Tauler, Multivariate curve resolution (MCR) from 2000: Progress in concepts and applications. Crit ReV Anal Chem (2006) 36: 163-176.

[68] W. Kessler, R.W. Kessler, Multivariate curve resolution: a method of evaluating the kinetics of biotechnological reactions. Anal Bioanal Chem (2006) 384: 1087-1095.

[69] M. Garrido, F.X. Rius, M.S. Larrechi, Multivariate curve resolution-alternating least squares (MCR-ALS) applied to spectroscopic data from monitoring chemical reactions processes. Anal Bioanal Chem (2008) 390: 2059–2066.

[70] W.H. Cassinelli, Multivariate curve resolution analysis applied to time-resolved synchrotron X-ray Absorption Spectroscopy monitoring of the activation of copper alumina catalyst. Catalysis Today (2014) 229 114–122.

[71] D.W. Mayo, F.A. Miller and R. W. Hannah. Course Notes on the Interpretation of Infrared and Raman Spectra, Wiley, Hoboken, NJ, (2004).

[72] R. Suryanarayanan, Determination of the Relative Amounts of Anhydrous Carbamazepine ($C_{15}H_{12}N_2O$) and Carbamazepine Dihydrate ($C_{15}H_{12}N_2O$ $2H_2O$) in a Mixture by Powder X-ray Diffractometry. Pharma Res (1989) 6(12): 1017–1024.

[73] R.K. Harris, P.Y. Ghi, H. Puschmann, D.C. Apperley, U.J. Griesser, R.B. Hammond, C. Ma, K.J. Roberts, G.J. Pearce, J.R. Yates, C.J. Pickard. Structural Studies of the Polymorphs of Carbamazepine, Its Dihydrate, and Two Solvates. Org Pro Res Dev (2005) 9: 902–910.

[74] K. Kipouros, K. Kachrimanis, I. Nikolakakis, S. Malamataris, Quantitative analysis of less soluble form IV in commercial carbamazepine (form III) by diffuse reflectance fourier transform spectroscopy (DRIFTS) and lazy learning algorithm. Analytica Chimica Acta (2005) 550(1–2): 191–198.

[75] W.W.L. Young, R. Suryanarayanan Kinetics of transformation of anhydrous carbamazepine to carbamazepine dihydrate in aqueous suspensions. J Pharm Sci (1991) 80: 496–500.

[76] M. Otsuka, T. Ohfusa, Y. Matsuda Effect of binders on polymorphic transformation kinetics of carbamazepine in aqueous solution. Colloid Surf B (2000) 17(3): 145–152.

[77] C. Bhugra, M.J. Pikal, Role of thermodynamic, molecular, and kinetic factors in crystallization from the amorphous state. J Pharm Sci (2008) 97: 1329–1349.

[78] V. Caron, L. Tajber, O. I. Corrigan, A. M. Healy, A comparison of spray drying and milling in the production of amorphous dispersions of sulfathiazole/polyvinylpyrrolidone and sulfadimidine/polyvinylpyrrolidone, Mol. Pharmaceutics. (2011) 8: 5320–542.

[79] M.L. Cheney, N. Shan, E. R. Healey, M. Hanna, L. Wojtas, M. J. Zaworotko, J. R. Sanchez-Ramos, Effects of crystal form on solubility and pharmacokinetics: a crystal engineering case study of lamotrigine. Cryst Growth Des 10 (2010) 394–405.

[80] Y.H. Kiang, E.A. Bercot, , Q. Wu, J. Liu, R.R. Milburn, D.E. Cohen, C.J. Borths, R.E. Saw, R.J. Staples, C. Davis, O.R. Thiel, Selection of a suitable physical form and development of a crystallization process for a PDE10A inhibitor exhibiting enantiotropic polymorphism. Org. Process Res Dev 19 (2015) 1849–1858.

[81] G. Dollo, P.L. Corre, M. Chollet, F. Chevanne, M. Bertault, J. L. Burgot, R. L. Verge, Improvement in solubility and dissolution rate of 1, 2-dithiole-3-thiones upon complexation with beta-cyclodextrin and its hydroxypropyl and sulfobutyl ether-7derivatives. J Pharm Sci 88 (1999) 889–895.

[82] P.T. Tayade, R. D. Kale, Encapsulation of water-insoluble drug by a cross-linking technique: effect of process and formulation variables on encapsulation efficiency, particle size, and in vitro dissolution rate. AAPS Pharm Sci (2004) 6: 112–119.

[83] A. Jayasankar, A. Somwangthanaroj, Z. J. Shao, N. Rodríguez-Hornedo, Cocrystal formation during cogrinding and storage is mediated by amorphous phase. Pharm Res (2006) 23: 2381–2392.

[84] P. Vishweshwar, J.A. Mcmahon, J.A. Bis, M.J. Zaworotko, Pharmaceutical co-crystals. J Pharm Sci (2006) 95: 499–516.

[85] E. Batchelor, J. Klinowski, W. Jones, Crystal engineering using co-crystallisation of phenazine with dicarboxylic acids. J Mater Chem (2000) 10: 839–848.

[86] C. Grossjohann, D.R. Serrano, K.J. Paluch, P. O'Connell, L. Vella-Zarb, P. Manesiotis, A.M. Healy, Polymorphism in sulfadimidine/4-aminosalicylic acid cocrystals: solid-state characterization and physicochemical properties. J Pharm Sci (2015) 104: 1385–1398.

[87] A. Fuliaş, G. Vlase, T. Vlase, L. M. Şuta, C. Şoica, I. Ledeți, Screening and characterization of cocrystal formation between carbamazepine and succinic acid. J Therm Anal Calori (2015) 121: 1–6.

[88] N. Schultheiss, A. Newman, Pharmaceutical cocrystals and their physicochemical properties. Cryst. Growth Des 9 (2009) 2950–2967.

[89] Y. Zao, H. Zu, J. Zhang, Enhanced dissolution and stability of adefovir dipivoxil by cocrystal formation. J Pharm Pharmacol 63 (2011) 483–490.

[90] D.P. McNamara, S.L. Childs, J. Giordano, A. Iarriccio, J. Cassidy, M.S. Shet, R. Mannion, E. O'Donnell, A. Park, Use of a glutaric acid cocrystal to improve oral bioavailability of a low solubility API. Pharm Res 23 (2006) 1888–1897.

[91] H. Furuta, S. Mori, Y. Yoshihashi, E. Yonemochi, H. Uekusa, K. Sugano, K. Terada,. Physicochemical and crystal structure analysis of pranlukast pseudo-polymorphs II: Solvate and cocrystal. J Pharm Biomed Anal (2015) 111: 44–50.

[92] H. Moradiya, M.T. Islam, G.R. Woollam, I.J. Slipper, S. Halsey, M.J. Snowden, D. Douroumis, Continuous cocrystallization for dissolution rate optimization of a poorly water-soluble drug. Cryst Growth Des 14 (2013) 189–198.

[93] S.J. Nehm, B. Rodriguez-Spong, N. Rodriguez-Hornedo, Phase solubility diagrams of cocrystals are explained by solubility product and solution complexation. Cryst Growth Des 6 (2006) 592-600.

[94] D. Bučar , Cryst, R.F. Henry, X. Lou, R. W. Duerst, L.R. MacGillivray, G. Z. Zhang, Cocrystals of caffeine and hydroxybenzoic acids composed of multiple supramolecular heterosynthons: Screening via solution-mediated phase transformation and structural characterization. Cryst Growth Des (2009) 9 1932-1943.

[95] M. Sopicka-Lizer, High-energy ball milling: Mechanochemical processing of nanopowders. CRC press LLC, New York, (2010) 7-108.

[96] A.V. Trask, W.S. Motherwell, W. Jones, Pharmaceutical cocrystallization: engineering a remedy for caffeine hydration. Cryst Growth Des (2005) 5: 1013–1021.

[97] J.H. An, F. Jin, H.S. Kim, H.C. Ryu, J. S. Kim, H. M. Kim, K. H. Kim, A. N. Kiyonga, K. Jung, Investigation of the polymorphic transformation of the active pharmaceutical ingredient clopidogrel bisulfate using the ionic liquid AEImBF4, Cryst. Growth Des (2016) 16: 1829–1836.

[98] S. Piqueras, L. Duponchel, R. Tauler, A. de Juan, Monitoring polymorphic transformations by using in situ Raman hyperspectral imaging and image multiset analysis. Anal Chim Acta (2014) 819: 15–25.

[99] Y. Otsuka, M. Yamamoto, H. Abe, M. Otsuka, Effects of polymorphic transformation on pharmaceutical properties of direct compressed tablets containing theophylline anhydrate bulk powder under high humidity. Colloid Surf B (2013) 102: 931–936.

[100] J. K. Maji, V. J. Shukla, Application of multivariate curve resolution alternating

least square (MCR-ALS) to the study of trikarshika formulation. Int J Pharm Sci (2016) 8: 238–243.

[101] Y. Otsuka, A. Ito, S. Matsumura, M. Takeuchi, S. Pal, H. Tanaka, Quantification of pharmaceutical compounds based on powder X-ray diffraction with chemometrics. Chem Pharm Bull (2016) 64: 1129–1135.

[102] Y. Otsuka, A. Ito, S. Matsumura, M. Takeuchi, H. Tanaka, Effect of hydroxypropyl cellulose and hydroxypropyl methylcellulose on carbamazepine polymorphic transformation; attenuated total reflectance-infrared spectroscopy and chemoinformatics analysis. Coll Polym Sci (2015) 293: 3471–3478.

[103] W. H. Cassinelli, L. Martins, A. R. Passos, S. H.Pulcinelli, C. V. Santilli, A. Rochet, V. Briois, Multivariate curve resolution analysis applied to time-resolved synchrotron X-ray absorption spectroscopy monitoring of the activation of copper alumina catalyst. Catalysis Today (2014) 229: 114–122.

[104] M. Garrido, F.X. Rius, M.S. Larrechi, Multivariate curve resolution-alternating least squares (MCR-ALS) applied to spectroscopic data from monitoring chemical reactions processes. Anal Bioanal Chem (2008) 390: 2059–2066.

[105] R. Tauler, Multivariate curve resolution applied to second order data. Chemom Intell Lab Syst (1995)30: 133-146.

[106] A. de Juan, R. Tauler, Multivariate curve resolution (MCR) from 2000: Progress in concepts and applications. Crit Rev Anal Chem (2006) 36: 163–176.

[107] W. Kessler, R.W. Kessler, Multivariate curve resolution: a method of evaluating the kinetics of biotechnological reactions. Anal Bioanal Chem (2006) 384: 1087–1095.

[108] S.J. Nehm, B. Rodríguez-Spong, N. Rodríguez-Hornedo, Phase solubility diagrams of cocrystals are explained by solubility product and solution complexation. Cryst Growth Des (2006) 6: 592–600.

[109] V.R.Vangala, P.S. Chow, M. Schreyer, G. Lau, R.B. Tan,. Thermal and in situ X-ray diffraction analysis of a dimorphic co-crystal 1: 1 caffeine-glutaric acid. Cryst Growth Des (2016) 16: 578–586.

[110] J. Jang, I.W. Kim, Poly (acrylic acid) to induce competitive crystallization of a theophylline / oxalic acid cocrystal and a theophylline polymorph. J Cryst Growth (2016) 434: 104–109.

[111] K. Guo, G. Sadiq, C. Seaton, R. Davey, Q. Yin, Co-crystallization in the caffeine/maleic acid system: lessons from phase equilibria, Cryst Growth Des (2009) 10: 268–273.

[112] W. Limwikrant, A. Nagai, Y. Hagiwara, K. Higashi, K. Yamamoto, K. Moribe Formation mechanism of a new carbamazepine / malonic acid cocrystal polymorph.

Int J Pharmaceut (2012) 431: 237–240.

[113] S. Basavoju, D. Bostrom, S. P. Velaga. Indomethacin–saccharin cocrystal: design, synthesis and preliminary pharmaceutical characterization. Pharm Res (2008) 25: 530–541.

[114] E. Gagniere, D. Mangin, F. Puel, J. P. Klein, O. Monnier, Cocrystal formation in solution: Inducing phase transition by manipulating the amount of cocrystallizing agent, J. Crystal Growth (2011) 316: 118–125.

[115] S.S. Kuduva, D.C. Craig, A. Nangia, G.R. Desiraju, Cubanecarboxylic acids. crystal engineering considerations and the role of CH-O hydrogen bonds in determining OH-O networks. J Am Chem Soc (1999) 121: 1936–1944.

[116] R. Suryanarayanan, Determination of the relative amounts of anhydrous carbamazepine ($C_{15}H_{12}N_2O$) and carbamazepine dihydrate ($C_{15}H_{12}N_2O$ $2H_2O$) in a mixture by powder X-ray diffractometry. Pharm Res (1989) 6: 1017–1024.

[117] R.G. Delaplane J.A. Ibers, An X-ray study of alpha-oxalic acid dihydrate $(COOH)_2$ $2H_2O$ and of its deuterium analogue, $(COOD)_2.2D_2O$: isotope effect in hydrogen bonding and anisotropic extinction effects. Acta Cryst (1969) B25: 2423–2437.

[118] N.L. Calvo, R.M. Maggio, T.S. Kaufman, A dynamic thermal ATR-FTIR/chemometric approach to the analysis of polymorphic interconversions. Cimetidine as a model drug. J Pharmaceut Biomed Anal (2014) 92: 90–97.

[119] N. Chieng, M. Hubert, D. Saville, T. Rades, J. Aaltonen, Formation kinetics and stability of carbamazepine−nicotinamide cocrystals prepared by mechanical activation, Cryst Growth Des (2009) 9: 2377–2386.

[120] S. Adzila, I. Sopyan, M. Hamdi, Mechanochemical synthesis of hydroxyapatite nanopowder: Effects of rotation speed and milling time on powder properties. Appl Mech Mater (2012) 110: 3639–3644.

[121] M.H. Fathi, E.M. Zahrani, Mechanical alloying synthesis and bioactivity evaluation of nanocrystalline fluoridated hydroxyapatite. J Crystal Growth (2009) 311: 1392–1403.

[122] A.V. Trask, J. van de Streek, W.S. Motherwell, W. Jones, Achieving polymorphic and stoichiometric diversity in cocrystal formation: Importance of solid-state grinding, powder X-ray structure determination, and seeding. Cryst Growth Des (2005) 5: 2233–2241.

[123] J. Chung, I.W. Kim, Effects of some polymeric additives on the cocrystallization of caffeine. J Crystal Growth (2011) 335: 106-109.